Purple membranes from *Halobacterium salinarum* as building blocks for nanobiotechnology: The importance of mechanical and thermal properties for matrix and surface applications

DISSERTATION

zur

Erlangung des Doktorgrades

der Naturwissenschaften

(Dr. rer. nat.)

dem Fachbereich Chemie

der Philipps-Universität Marburg

vorgelegt von

DANIEL CHRISTOPHER RHINOW

aus Frankfurt am Main

Marburg an der Lahn 2008

Erstgutachter: Prof. Dr. Norbert A. Hampp

Zweitgutachter: Prof. Dr. Lars-Oliver Essen

Einzelne Teile dieser Arbeit wurden vorab veröffentlicht:

1.) Rhinow, D.; Hampp, N. A.
Sugar-Induced Blue Membrane: Release of Divalent Cations during Phase Transition of Purple Membranes Observed in Sugar-Derived Glasses
J. Phys Chem B **2007**, *112*, 4613.

2.) Rhinow, D.; Hampp, N. A.
Forming Microstructured Alkanethiol Self-Assembled Monolayers on Gold by Laser Ablation
IEEE Trans. Nanobiosci. **2006**, *5*, 188.

3.) Rhinow, D.; Hampp, N. A.
Solid-Supported Multicomponent Patterned Monolayers
Adv. Mater. **2007**, *19*, 1967.

4.) Neebe, M.; Rhinow, D.; Schromczyk, N.; Hampp, N. A.
Thermochromism of Bacteriorhodopsin and Its pH Dependence
J. Phys. Chem. B, **2008** *112*, 6946.

5.) Rhinow, D.; Hampp, N. A.
Light- and pH-Dependent Conformational Changes in Protein Structure Induce Strong Bending of Purple Membranes - Active Membranes Studied by Cryo-SEM
J. Phys. Chem. B ***2008,*** *112, 13116.*
- selected for cover image for *J. Phys. Chem. B 112, Vol. 42* (see next page)

JPCBFK

VOLUME 112
OCTOBER 16, 2008
NUMBER 41
http://pubs.acs.org/JPCB

THE JOURNAL OF PHYSICAL CHEMISTRY B

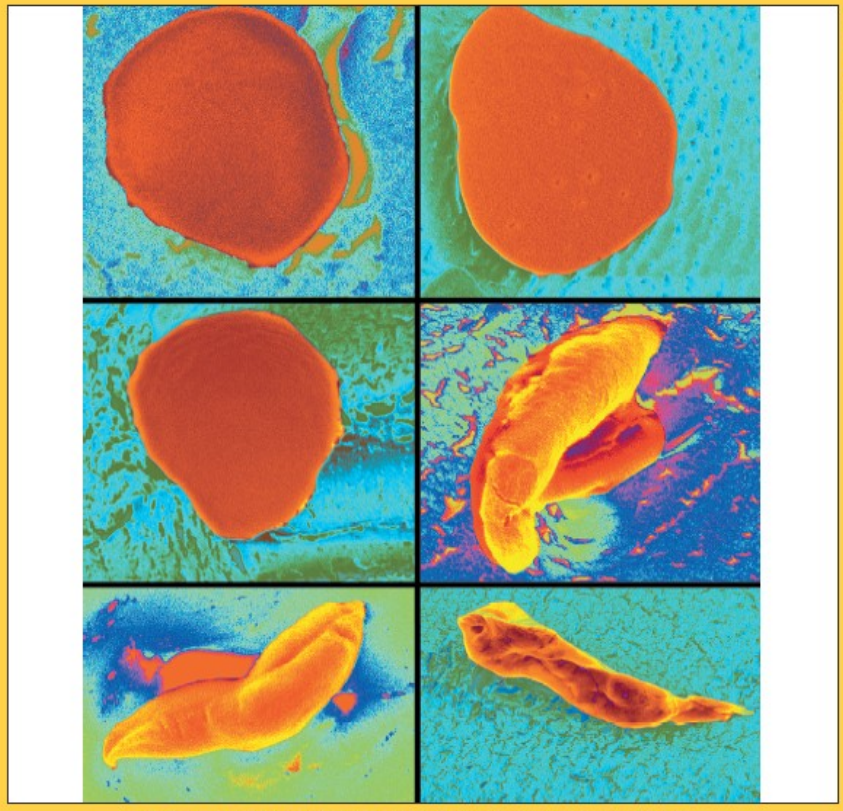

Illumination-Dependent Topology of PM Analyzed by cryo-SEM
(see page XA)

SOFT CONDENSED MATTER AND BIOPHYSICAL CHEMISTRY

PUBLISHED WEEKLY BY THE AMERICAN CHEMICAL SOCIETY

MITTELMEERISCH

Ach, aus den Archipelagen
da im Orangengeruch
selbst die Trümmer sich tragen
ohne Tränen und Fluch,

strömt in des Nordens Düster,
Nebel- und Niflheim,
Runen- und Lurengeflüster
mittelmeerisch ein Reim:

Schließlich im Grenzenlosen
eint sich Wahrheit und Wahn,
wie in der Asche der Rosen
schlummert der Kiesel, Titan,

dein aber ist das Schreiten,
dein die Grenze, die Zeit,
glaube den Ewigkeiten
fordre sie nicht zu weit,

aus ihrer halben Trauer,
rosen- und trümmerschwer,
schaffe den Dingen Dauer -
strömt es vom Mittelmeer.

(Gottfried Benn)

INHALTSVERZEICHNIS

ZUSAMMENFASSUNG DER DISSERTATION 8

1. INTRODUCTION 12

1.2 THE PURPLE MEMBRANE OF *HALOBACTERIUM SALINARUM* 12

1.2.1. Structure of purple membrane and Bacteriorhodopsin 12

1.2.2. The photocycle of Bacteriorhodopsin – molecular basis of enzyme function 14

1.2.3. Blue membrane formation and cation binding by Bacteriorhodopsin 16

1.3. IMMOBILIZATION OF PROTEINS IN SUGAR-DERIVED GLASSES 18

1.4. SOLID-SUPPORTED NANOBIOTECHNOLOGY 18

1.4.1. Immobilization of PM on self-assembled monolayers (SAMs) of alkanthiols on gold 18

1.5. MEMBRANE CURVATURE AND PROTEIN FUNCTION 20

1.5.1 The importance of membrane curvature in cell biology 20

1.5.2. Bending of purple membranes during photocycle 21

1.5.3. Cryogenic high-resolution scanning electron microscopy (Cryo-SEM) 22

2. MATERIALS AND METHODS 23

2.1. PURPLE MEMBRANE PREPARATION 23

2.1.1. PM purification 23

2.1.2. PM films 23

2.2. SPECTROSCOPY 23

2.2.1. UV-Vis spectroscopy 23

2.2.2. FT-IR spectroscopy 23

2.3. SELF-ASSEMBLED MONOLAYERS (SAMS) OF ALKANETHIOLS ON GOLD 24

2.3.1. Preparation of template stripped gold (TSG) 24

2.3.2. Preparation of alkanethiol SAMs 24

2.3.3. Patterning of SAMs via submerged laser ablation (SLAB) 24

2.3.4. Optical microscopy 25

2.3.5. Cyclic voltammetry 26

2.4. STRUCTURAL ANALYSIS *26*

2.4.1. Atomic force microscopy (AFM) *26*

2.4.2. Scanning electron microscopy of SAMs *26*

2.4.3. cryo-SEM of PM *26*

3. RESULTS AND DISCUSSION **28**

3.1. THERMOCHROMISM OF SUGAR-EMBEDDED PURPLE MEMBRANES *28*

3.1.1. Matrix-dependent thermochromism of BR -The sugar-induced blue membrane (SIBM) *28*

3.1.2. The role of water and divalent cations *34*

3.1.3. Model for SIBM *36*

3.1.4. Thermal reconversion of SIBM to PM monitored by visible spectroscopy *40*

3.1.5. Differences in secondary structure of PM and SIBM *41*

3.2. SOLID-SUPPORTED ASSEMBLY OF PURPLE MEMBRANES *43*

3.2.1. Thermochromism of solid-supported PM *43*

3.2.2. Adsorption of PM on SAMs *45*

3.2.3. Fabrication of structured self-assembled monolayers of alkanethiols *48*

3.3. MECHANICS OF FREELY-SUSPENDED PURPLE MEMBRANES *55*

3.3.1. Light-induced bending of purple membranes analyzed by cryo-SEM *55*

3.3.2. pH-induced bending of mutant D85T *58*

3.3.3. Mechanistic basis of purple membrane bending *60*

3.3.4. Membrane bending due to opening of the EC half-channel *63*

3.3.5. The purple membrane is a supramolecular actuator *64*

REFERENCES **65**

ABBREVIATIONS **78**

DANKSAGUNGEN **80**

CURRICULUM VITAE **81**

Zusammenfassung der Dissertation

Einleitung und Fragestellungen

Die licht-getriebene Protonenpumpe Bakteriorhodopsin (BR) aus dem halophilen Organismus *Halobacterium salinarum* [Oesterhelt, Stockenius, 1971] ist das Schlüsselprotein der halobakteriellen Photosynthese. BR gehört zu den wenigen Membranproteinen, die in ihrer nativen Umgebung mit spektroskopischen und strukturanalytischen Verfahren eingehend untersucht werden konnten. In seiner nativen Lipidumgebung ist BR in den so genannte Purpurmembranen (PM) zu finden, die zu 75 % aus BR und 25 % aus Lipiden bestehen und zu der seltenen Klasse natürlich vorkommender Membranprotein-2-D-Kristalle gehören. In der PM besitzt BR eine beeindruckende thermische Stabilität [Shen et al., 1993] und ist vergleichsweise unempfindlich gegenüber einer Vielzahl von chemischen und physikalischen Einflüssen. Die funktionelle Vielfalt dieses halobakteriellen Retinalproteins macht es zu einem viel versprechenden Material für eine Reihe von technischen Anwendungen, die auf die photochromen und photoelektrischen Eigenschaften von BR zurückgreifen [Hampp, 2000].

Die meisten technischen Anwendungen von BR und PM erfordern Matrixeinbettung oder Immobilisierung der PM auf einem festen Substrat. In diesem Zusammenhang stellen sich folgende wichtigen Fragen, die im Rahmen der vorliegenden Arbeit untersucht wurden:

-Welchen Einfluss hat die Matrixeinbettung auf die Funktion von BR? Diese kann über seine spektralen Eigenschaften gut detektiert werden. Gibt es Matrixmaterialien, die in spezifischer Weise mit dem Protein wechselwirken?

-Auf welchem Weg können Oberflächen strukturiert werden die zur ortsselektiven Immobilisierung von PMs auf diesen Oberflächen geeignet sind? Hierbei ist zu bedenken, dass wegen der Größe der PMs die Brown'sche Molekularbewegung praktisch keine Rolle mehr spielt.

-Der Photozyklus von BR wird durch die photoinduzierte all-trans- nach 13-cis-Isomerisierung des Retinalchromophors initiiert. Die nachfolgenden thermisch kontrollierten Reaktionen sind mit einer Reihe von Konformationsänderungen im Proteingerüst verbunden, die teils auch zu transienten Formänderungen des BRs führen. Da sich in jeder PM tausende, durch den kristallinen Verbund stark gekoppelter BR-Moleküle in undirektionaler lateraler Anordnung befinden, führen kollektive Konformationsänderungen der aktiven BR-Moleküle zu einer Änderung der Geometrie der Gesamtmembran. Gibt es transiente oder permanente Abweichungen von der planaren Form der PM? Welche Implikationen ergeben sich daraus für die Anwendung von PM an Grenzflächen, die einen Symmetriebruch gegenüber der nativen wässrigen Umgebung bedeuten, wie z.B. an einer Oberfläche?

PM in Zuckermatrizen - Thermochrome Änderungen

Amorphe Zuckergläser sind in der Lage das native wässrige Millieu zu imitieren und Proteine auch in annähernd wasserfreien Präparationen funktionell aktiv zu halten [Dubochet et al., 1988; Crowe et al., 1984]. Wichtige funktionelle Einblicke in Struktur und Funktion von BR wurden mittels cryo-TEM an zuckerimmobilisierter PM gewonnen [Henderson et al., 1990; Grigorieff et al. 1996; Kimura et al., 1997]. Allerdings konnte im Rahmen dieser Arbeit gezeigt werden, dass Zuckermatrizen unter bestimmten Bedingungen stark mit PM wechselwirken. PM wurde in diversen Zuckergläsern immobilisiert und die temperaturabhängigen Protein-Matrix Wechselwirkungen untersucht. Dabei wurden thermochrome Änderungen beobachtet, die sich von dem in einer anderen Arbeit analysierten Thermochromismus in Lösung [Neebe et al., 2008] unterscheiden. Es konnte gezeigt werden, dass sich unabhängig von der Natur der verwendeten Zucker oberhalb einer Grenztemperatur von $T > 60°C$ eine blaue Membran bildet, die so genannte „Sugar-Induced Blue Membrane“ (SIBM). Aufbauend auf UV-Vis- und FTIR-spektroskopische Analysen wurde ein Modell für die SIBM-Bildung entwickelt. Demnach führen Phasenübergänge in der PM bei $T > 60°C$ zur Freisetzung vorher fest gebundener divalenter Kationen. Die Kohlenhydrat-Moleküle, die schwache Chelatbildner sind, sorgen für eine effektive Komplexierung und Delokalisierung der freigesetzten Kationen in der

Zuckermatrix. Divalente Kationen sind mitverantwortlich für die die spektralen Eigenschaften des BRs. Das Spektrum der kationenfreien PM verschiebt sich bathochrom.

Strukturierung von Alkanthiol-Self-Assembled-Monolayers (SAMs) auf Gold zur Adsorption von PM

Alkanthiole sind vielseitige Bausteine der oberflächengebundenen Nanobiotechnik [Love et al., 2005]. Sie erlauben die Funktionalisierung von Metalloberflächen und ermöglichen dadurch spezifische und nicht-denaturierende Wechselwirkungen mit Biomolekülen. Alkanthiole mit geladenen Endgruppen sind in der Lage, auch große Membranproteinkomplexe durch elektrostatische Wechselwirkungen zu adsorbieren [Valiokas et al. 2006]. Aufgrund ihrer hohen Masse zeigen PMs vernachlässigbare Diffusion, so dass ladungsvermittelte Adsorption an Oberflächen ein attraktives Verfahren zur Immobilisierung vom PM ist.

Es wurde gezeigt, dass sich die von Valiokas et al. beschriebene Methode der Adsorption von Proteinen an positiv geladenen SAMs auch auf PMs anwenden lässt, die bei physiologischen pH-Werten eine negative Oberflächenladung besitzen. Funktionalisiert man Goldoberflächen dagegen mit negativ geladenen SAMs, so bestimmt der Salzgehalt des Puffers ob die Adhäsionseigenschaften der Oberfläche attraktiv oder repulsiv für PM sind.

Zur Strukturierung der Alkanthiol-SAMs wurde ein Verfahren entwickelt, das sich bestens für die Herstellung monolagiger Strukturen im Mikrometerbereich eignet, die so genannte „Submerged Laser Ablation“ (SLAB). Dabei werden aus einem Alkanthiol-SAM auf Gold mittels energiereicher Laserpulse Alkanthiolmoleküle thermisch herausgelöst und durch andere Alkanthiole ausgetauscht. Ein Vorzug dieses Verfahren ist, dass der Alkanthiol-Austausch unmittelbar erfolgt. Dies wird erreicht, indem eine bestehende Monoschicht mit einer Lösung des einzuschreibenden Alkanthiols überschichtet wird. Die durch Laserablation entstandenen Freistellen werden also sofort durch Alkanthiol-Moleküle aus der überstehenden Lösung aufgefüllt. Die Überschichtung mit Lösung besitzt den Vorteil, dass auf diese Weise eine Kontamination der Oberfläche mit Goldpartikeln verhindert wird, die sonst bei der Strukturierung des Goldsubstrates entstehen. Die strukturierten SAMs wurden mit Rasterelektronenmikroskopie (SEM) und Cyclovoltammetrie (CV) untersucht.

Licht- und pH-abhängige Krümmung der Purpurmembran

Für die PM hatten sich in der Vergangenheit spektroskopische Hinweise auf eine Krümmung der PM während des Photozyklus ergeben. Im Hinblick auf die Verwendung von PM in der Nanobiotechnologie, in der Wechselwirkungen zwischen Oberflächen und daran angekoppelten Biomolekülen eine zentrale Rolle spielen, ist eine Kenntnis der Krümmungseigenschaften der PM natürlich von großer Bedeutung. Im Rahmen dieser Arbeit konnte die funktionelle Krümmung der PM während des Photozyklus zum ersten Mal mit strukturanalytischen Methoden direkt nachgewiesen werden. Als Methode kam hierbei die hochauflösende cryo-Rasterelektronenmikroskopie (cryo-SEM) zum Einsatz. Diese erlaubt die strukturelle Charakterisierung frei-suspendierter PMs. Durch Verwendung der Mutante PM-D96N, deren Photozyklus einen langlebigen M_2-Zustand aufweist, konnte gezeigt werden, dass eine Konformationsänderung des BR-Moleküls im M_2-Zustand für die Krümmung der Membranen während des Photozyklus verantwortlich ist.. Während die vorgelagerten Photozyklus-Intermediate mit vergleichsweise kleinen Umlagerungen im Proteingerüst verbunden sind, erfolgt im M_2-Zustand die Öffnung des cytoplasmatischen Kanals. In der PM befinden sich tausende stark gekoppelter BR-Moleküle in einer unidirektionalen lateralen Anordung. Dadurch summieren sich die kollektiven nanoskaligen Konformationsänderung auf und führen zu einer makroskopischen Krümmung der Membran. Eine durch den pH-Wert induzierte Krümmung der PM konnte anhand der Mutante PM-D85T demonstriert werden. Die eingeführte Mutation verändert den pK_a-Wert wichtiger funktioneller Gruppen in der Retinalbindungstasche. So lässt sich durch den Wechsel vom Neutralen ins Alkalische die Schiff-Base deprotonieren, was im BR-Molekül zu den gleichen Konformationsänderungen führt, wie sie im M_2-Zustand des Photozyklus auftreten. Die Folge ist auch hier eine makroskopische Krümmung der PM.

Aufbauend auf diesen Experimenten wurde ein verallgemeinertes Modell für die mechanische Kopplung von Zuständen auf Einzelmolekülebene mit makroskopisch nachweisbaren Veränderungen der PM-Topologie entwickelt. In der vorliegenden Arbeit konnte gezeigt werden, dass PM ein supramolekularer mechanischer Schalter ist, der je nach Mutante durch Licht und Änderungen des pH-Werts aktiviert werden kann.

1.2 The purple membrane of *Halobacterium salinarum*

1.2.1. Structure of purple membrane and Bacteriorhodopsin

Membrane proteins are involved in all elementary processes of life. They provide the functional framework for energy conversion and maintain the transport of essential molecules and ions across the cell membrane. The number of known membrane protein structures is very small compared to their important role they play in cell biology. Structural analysis as well as physico-chemical investigation of membrane proteins is hampered due to the amphiphilic nature of membrane proteins. Full activity is observed only in their native membrane environment. This requirement limits the number of methods suitable for the biophysical characterization of membrane proteins.

Bacteriorhodopsin (BR) is a light-driven proton pump and the key protein in halobacterial photosynthesis [Oesterhelt, Stockenius, 1971; Haupts et al., 1999]. It is found in the archaeon *Halobacteriium salinarum*, a halophilic organism which lives under extreme conditions, and is found for example in salterns as well as in salt lakes. In its native host BR trimers arrange into a 2-D crystalline lattice of p3 symmetry, the so called purple membranes (PMs) which comprises BR and lipids only. BR is among the best studied membrane proteins. The great interest in BR is threefold. At first, BR is the other important photosynthetic system in nature besides the well-known chlorophyll-based photosystem of green plants. Secondly, BR belongs to the important class of seven helix membrane proteins, and shares deep homologies with other retinal proteins as well as G-protein-coupled receptors (GPCRs). At third, because of its astonishing stability against thermal and chemical stress BR is an excellent candidate for a variety of technical applications which make use of the photochromic and photoelectric properties of BR [Hampp, 2000].

The first structural model of BR with atomic resolution was obtained by electron crystallography [Henderson et al., 1990] which was subsequently refined [Grigorieff et al., 1996], and extended to complete resolution of the formerly hardly resolved BR surface

[Kimura et al., 1997]. In the following years 3-D crystallization succeeded to give crystals suitable for x-ray diffraction, and several atomic models with increasing resolution were published which gave further insights into BR structure and function. Among the structures obtained is BR in its trimeric assembly including lipids (Essen et al., 1998), and an atomic model of BR acquired from lipidic cubic phases (Luecke et al., 1999).

The 3-D structure of BR is schematically shown in figure 1. Fig. 1A shows the trimeric assembly of BR monomers as seen from the extracellular (EC) side. The major part of BR's secondary structure consists of seven α-helixes which span the whole membrane (Fig. 1B), and are connected by short loops. An antiparallel β-sheet is found in the B-C loop.

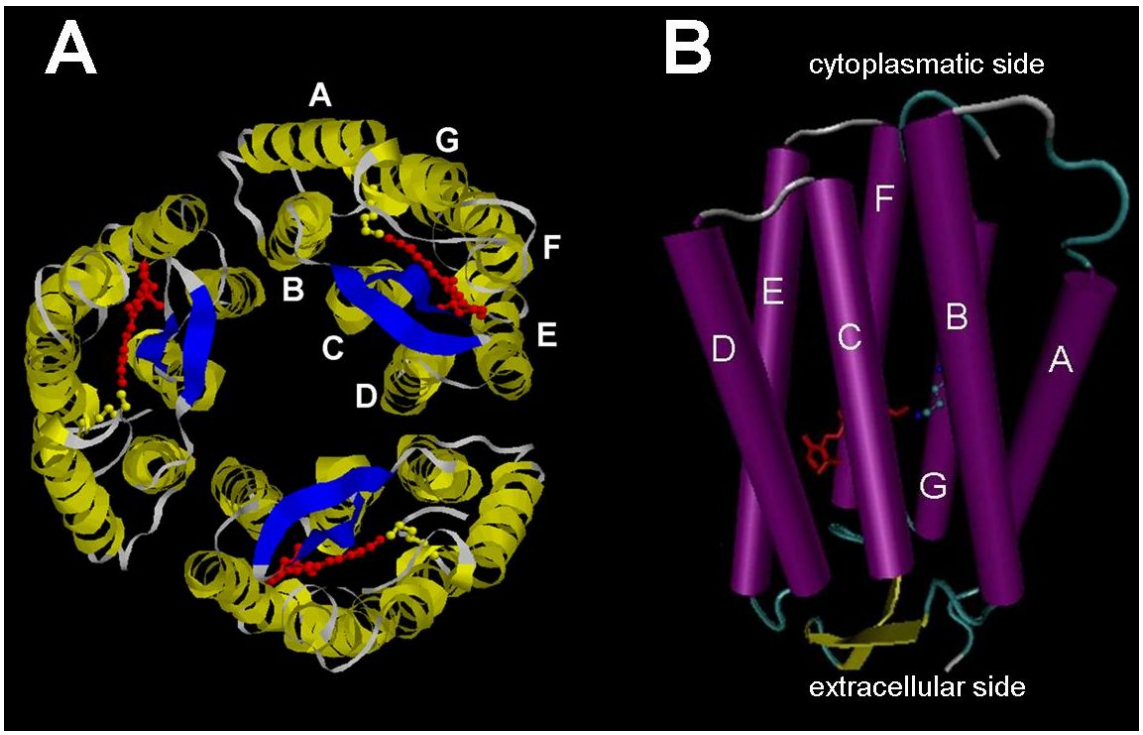

Figure 1. Structural model of bacteriorhodopsin (BR). (left) Assembly of BR trimers in PM, viewed from the extracellular side (coordinates obtained from PDB entry 1BRR) [Essen et al., 1998]. Each monomer comprises seven transmembrane helices (labeled A to G) which are interconnected by amino acid loops. The B-C loop contains a β-sheet structure (blue color). Retinal (red color) is bound to the protein backbone via a Schiff base to lysine-216. (right) View to the BR helices from the side.

1.2.2. The photocycle of Bacteriorhodopsin – molecular basis of enzyme function

BR belongs to the large class of retinal proteins which all share similarities in structure and protein function. In the core of BR a single retinal molecule is covalently linked to K216 via a Schiff base linkage which is protonated (PSB) in the initial state. The spectral properties of the chromophore are regulated by essential amino acid residues in the so-called retinal binding pocket (Fig. 2). The positively charged PSB interacts strongly with other charged groups, among them D85, D212, and R82 (Fig. 2A). The carotene tail of retinal is embedded in a lipohilic environment provided by aromatic amino acids (Fig. 2B).

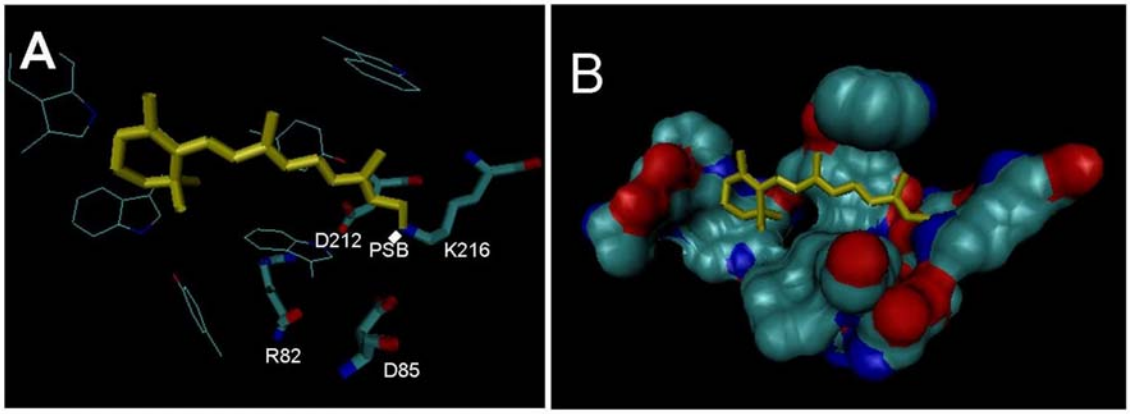

Figure 2 The retinal binding pocket of BR. (A) Labelled here are amino acid residues which interact directly or indirectly with the PSB (B) Molecular surface of the retinal binding pocket. The carotene tail of the chromophor is embedded in a hydrophobic environment maintained by aromatic amino acids.

Upon absorption of visible light BR performs a photocycle starting from the initial state B_{570} which is intensely purple colored. The initial step of the photocycle includes the rapid isomerization of retinal from all-trans to 13-cis (Fig. 3) which is completed within 500 fs [Haupts et al., 1999].

Furthermore, the strong polarization of the chromophore due to photon absorption results in the transfer of polarization energy to the protein framework which provides additional energy for the following steps of the photocycle. Except the first step all further reactions of the photocycle comprise thermal conversions which finally lead to the translocation of a proton across the membrane. While all thermal conversions are reversible in principle the transition from the M^{I} to the M^{II} state is considered irreversible.

Both states are undistinguishable in the UV spectrum but structural analysis has given evidence for a large-scale conformational change during the transition to M^{II} [Subramaniam, Henderson, 2000; Subramaniam et al., 1999; Sass et al., 1997] which ensures unidirectional proton transport.

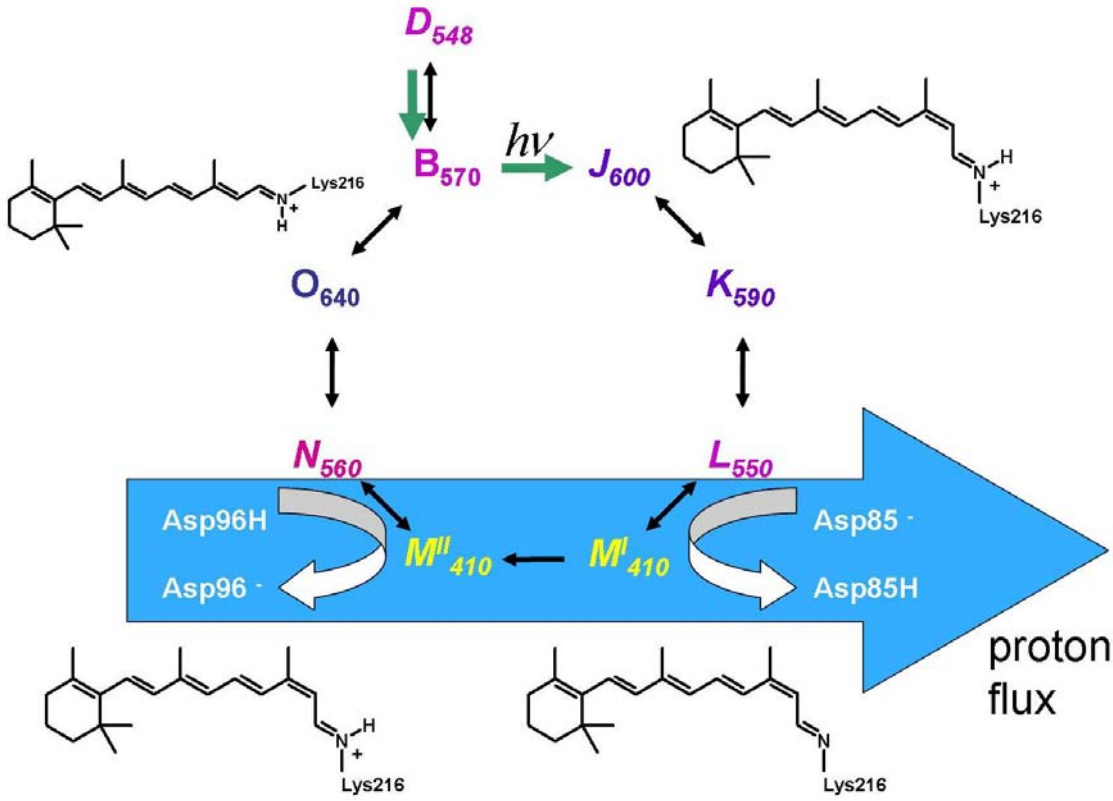

Figure 3 The photocycle of Bacteriorhodopsin. Absorption of green light by retinal starts the photocycle, and leads to trans-cis isomerization around the C_{13}=C_{14} double bond, starting from all-trans retinal in the ground state (B_{570}). Intermediates which comprise 13-cis retinal are marked in italics. Except the first transition, which is triggered photochemically, all reactions are thermal conversions. During the L → M^I transition the Schiff-Base proton is transferred to Asp85. The M^I → M^{II} transition is accompanied by a large-scale conformational change which makes this step of the photocycle irreversible. The Schiff base is reprotonated in the N state via proton transfer from Asp96H. After cis→trans reisomerization of retinal in the O state the initial state B is recovered.

1.2.3. Blue membrane formation and cation binding by Bacteriorhodopsin

Several forms of blue membrane have been described. Acidification of PM as well as cation removal result in a significant bathochromic shift of the absorption spectrum, leading to the formation of acid blue membrane (ABM) [Mowery et al., 1979; Fischer et al., 1981; Kimura et al., 1984] and cation-free blue membrane (CFBM). [Chang et al. 1985; Liu, Ebrey, 1987; Zhang et al., 1993; Birge et al., 1996] Treatment of PM with low concentrations of sodium dodecyl sulfate leads to the so-called detergent-induced blue membrane (DIBM) [Padros et al., 1984] Another form of blue membrane is the laser-induced blue membrane (LIBM) which is observed upon irradiation of PM suspensions with intense laser pulses [Czege, Reinisch, 1991; Masthay et al., 2002; Fischer, Hampp, 2005] In all cases molecular changes take place which cause that the chromophore environment is altered and a spectral shift from purple to blue results.

Albeit several high-resolution structures of BR and its trimeric assembly have been published [Essen et al., 1998; Luecke et al., 1999] the exact location of the cation binding sites has not yet been determined.

Two lines of argumentation have arisen about the cation location. One approach explains the cation-mediated color regulation of BR in terms of Guy-Chapman theory [Szundi, Stockenius, 1989]. According to this hypothesis cations are unspecifically bound to the membrane surface by electrostatic interactions with negatively charged residues, and mediate the surface pH. However, several studies give evidence for the existence of specific cation binding sites within the BR molecule, and their importance for maintaining function and stability of PM [Jonas, Ebrey, 1991; Zhang et al., 1992; Yang, El-Sayed, 1995; Tuzi et al. 1999; Heyes, El-Sayed, 2001]. In a recent electron paramagnetic resonance (EPR) study Eliash et al. analyzed the interaction of Mn^{2+} with several spin-labeled BR mutants [Eliash et al., 2001]. Using mutant E74C, they found that the highest-affinity binding site of Mn^{2+} is located within a radius of 9.8 Å around position 74, and claimed the existence of a high-affinity cation binding site in the vicinity of the extracellular B-C loop. In native BR the B-C loop consists of an antiparallel β-sheet (marked in yellow in Fig. 4). The previous suggestion is supported by a recently published x-ray structure of blue

membrane [Okumura et al., 2005]. The authors observed that in the blue form of BR the B-C loop as well as the glycolipid moiety in the central part of the BR trimer is highly disordered. They speculated that both, the B-C loop and the glycolipid in close proximity together form a cation binding site and, vice versa, the β-sheet motive of the B-C loop is maintained by cation binding.

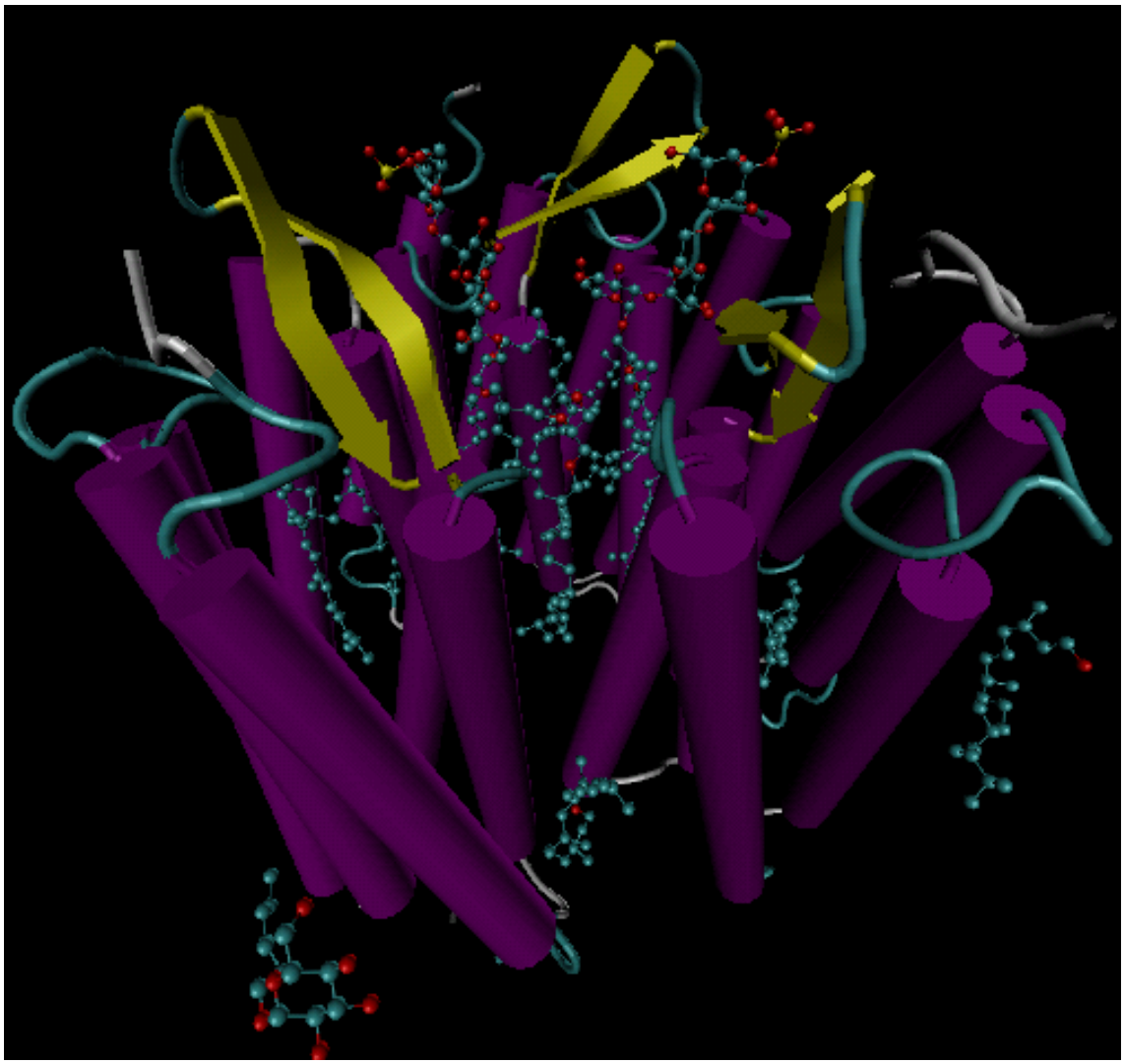

Figure 4 The trimeric assembly of BR, including lipid molecules (PDB entry 1BRR). View from the extracellular side. The interior space between BR trimers is filled with glycolipids.

1.3. Immobilization of proteins in sugar-derived glasses

Immobilization of biomolecules in sugar-derived glasses plays an important role in particular in structural biology, nanobiotechnology, and in pharmaceutical applications [Dubochet et al., 1988; Crowe et al., 1984; Carpenter et al. 1987; Crowe et al., 1992; Singer, Lindquist, 1998; Carninci et al., 1998; Kaushik, Bhat, 2003]. For example, in protein structure determination by cryo-electron microscopy, vitrification of samples is a key step, protecting them against drying and beam damage [Dubochet et al. 1988]. In the case of membrane proteins seminal insights into structure and function have been obtained from sugar-embedded samples [Henderson et al., 1990; Grigorieff et al. 1996; Kühlbrandt et al., 1994; Kimura et al., 1997; Gonen et al., 2005]. Sugar glasses mimic the native aqueous milieu. However, it became obvious that carbohydrate-protein interactions in sugar matrices have an effect on protein structure and function. The highly viscous environment affects protein dynamics seriously [Hagen et al., 1995; Fenimore et al., 2002; Fraunfelder et al. 2006].

In this thesis the thermochromic changes of sugar embedded-PM is analysed (chapter 3.1.). The so called sugar-induced blue membrane [Rhinow, Hampp, 2007] is an example for strong protein-matrix interactions.

1.4. Solid-supported nanobiotechnology

1.4.1. Immobilization of PM on self-assembled monolayers (SAMs) of alkanthiols on gold

Self-assembled monolayers of alkanethiols (SAMs) on gold are important tools for nanotechnology [Love et al. 2005]. Essential parts of nanotechnology employ solid-supported architectures, in particular gold surfaces. Alkanethiol SAMs provide a versatile connection between the metallic substrate and functional building blocks (Fig. 5). The choice of suitable end groups enables the immobilization of biomolecules by means of physical forces as well as chemical bonding.

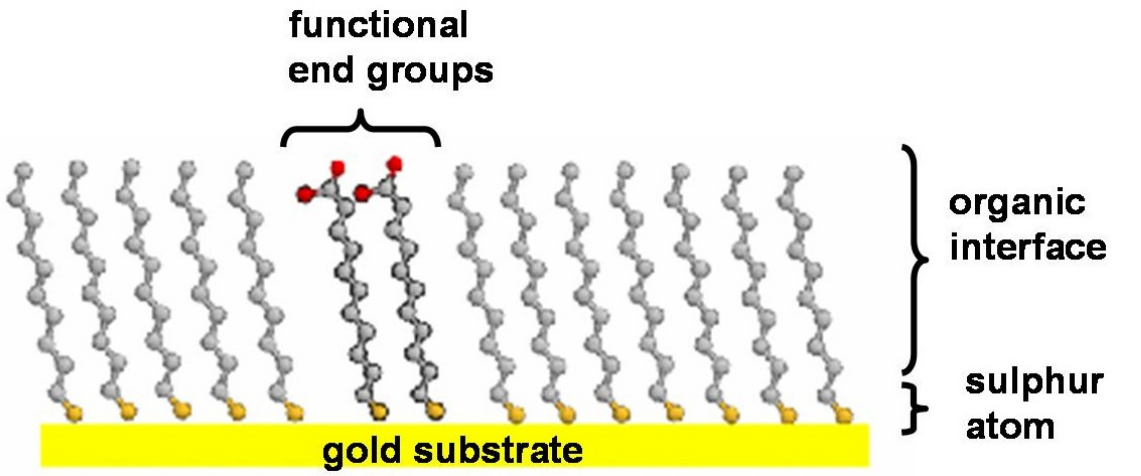

Figure 5 Alkanethiol SAMs on gold. Functional end groups serve as specific capture ligands, in particular for the immobilization of biomolecules.

The immobilization of membrane proteins on surfaces remains a challenge because proper function is only retained in a near-native lipid environment. Adsorption to patterned alkanethiol SAMs has emerged as a promising approach for the immobilization of large membrane protein complexes onto surfaces [Valiokas et al., 2006].

But the development of methods for the patterning of alkanethiol SAMs is as well a key challenge in the field of biochip fabrication. Micron sized adsorption sites have to be fabricated in the case of PM. UV-lithography is a well established patterning scheme for SAMs [Huang et al., 1994; Behm et al. 1996; Anderson et al., 2006] but less suitable for smaller series. Mechanical methods for patterning of SAMs have been developed and overcome this problem. Among them micro contact printing [Kumar, Whitesides, 1993] (μCP) and dip-pen nanolithography [Piner et al., 1999] are the most prominent ones. Although with μCP spatial resolutions better than 100 nm have been achieved it is difficult to use μCP for multi step patterning procedures. Dip-pen nanolithography in turn is limited in speed. Attempts have been made to increase the speed of dip-pen methods by massive parallelisation [Salaita et al., 2006]. E-beam technology has attracted interest of several groups [Lercel et al., 1994; Gölzhäuser et al., 2001] and high-resolution structures were realized, but the equipment is very costly. Other techniques like x-ray lithography [Heister

et al., 2001], ink-jet printing [Pardo et al., 2003; Bietsch et al. 2004], nanografting [Xu et al., 1999] and even near-field lithography [Sun et al., 2002] were explored for this challenging task. Direct laser patterning of alkanethiols is a newer alternative patterning method [Shadnam et al., 2004; Rhinow, Hampp, 2006]

A method for the patterning of alkanethiol SAMs is presented in chapter 3.2.3. . The procedure has been named submerged laser ablation (SLAB) [Rhinow, Hampp, 2007 (2)], and enables the fabrication of large-area patterned SAMs suitable for PM adsorption.

1.5. Membrane curvature and protein function

In their native host both sides of PMs are in touch with an aqueous environment, and are able to perform large-scale conformational changes without restriction by a solid support. Therefore, apart from being an interesting research topic on its own, detailed knowledge of the mechanics of freely-suspended PM is of great importance in surface-based applications of PM. The occurrence of transient or permanent bending of PMs due to protein function would have serious consequences for applications in which the topology of PM is constrained, for example in rigid matrixes or on surfaces. Therefore, proper knowledge about the mechanical properties of PM is a prerequisite for nanobiotechnological applications.

1.5.1 The importance of membrane curvature in cell biology

A recent topic in cell biology is the analysis of membrane curvature and its mechanical coupling to specialized membrane proteins which induce membrane bending due to their shape. Cell organelles like endoplasmatic reticulum, the Golgi apparatus, caveoli, and inner mitochondria membranes comprise highly-curved membrane topologies [Voeltz, Prinz, 2007; Zimmerberg, Kozlov, 2006; Farsad, De Camilli, 2003; Bauer, Pelkmanns, 2006; Voeltz et al., 2006; Martens et al., 2007; Hu et al. 2008]. In all cases special proteins provide a scaffold for maintaining membrane curvature.

1.5.2. Bending of purple membranes during photocycle

Another field of biophysical research which addresses the issue of membrane bending is the study of active membranes at work [Prost et al. 1996; Prost et al., 1998; Manneville et al., 1999; Ramaswamy et al., 2000; Manneville et al., 2001; Gov, 2004; Lin et al. 2006; Giahi et al. 2007] In the case of PM membrane bending has been claimed to occur during the photocycle [Czege, Reinisch, 1987; Czege, Reinisch, 1991]. Based on early light scattering experiments, the authors postulated that transient asymmetries in charge distribution are responsible for membrane bending which occurs as a result of the proton transport across the membrane. However, the initial work on this subject was done before high-resolution structural data were available for BR, and the conclusions were solely drawn from light-scattering studies. Roughly ten years later, a study employed modern electro-optical techniques as well as mutant PM-D96N to re-examine the question of purple membrane bending [Porschke, 2003]. In the mean time, several high-resolution 3-D structures of BR had been published [Grigorieff et al., 1996; Kimura et al., 1997; Essen et al., 1998; Luecke et al. 1999; Sass et al., 2000; Subramaniam, Henderson, 2000]. The author concluded [Porschke, 2003] that PM experiences bending related to M-state formation during the photocycle. Not an asymmetric charge distribution between the different sides of the PM but a large-scale conformational change in BR tertiary structure, which was observed in atomic models obtained by electron crystallography [Subramaniam, Henderson, 2000], was assigned responsible for the mechanical changes. However, a direct proof of purple membrane bending by means of imaging techniques has not yet been given.

Electron crystallography [Kühlbrandt et al. 1994; Grigorieff et al., 1996; Kimura et al., 1997; Gonen et al. 2005] as well as atomic force microscopy (AFM) [Müller et al., 1995; Müller, Engel, 1999; Oesterhelt et al., 2000; Sapra et al., 2006] make use of two-dimensional crystals of membrane proteins, and have contributed much to the elucidation of their structure and function, particularly in the case of BR. However, with the exception of electron microscopy by means of holey films, both methods require solid supports which confine the membranes to a flat topology. X-ray diffraction has been used to study membrane fluctuations, but employs solid-supported membranes as well [Shen et al., 1993; Koltover et al., 1998; Koltover et al., 1999; Salditt et al., 1999; Müller et al, 1999 (1);

Salditt et al, 2000]. Membrane fluctuations, driven by active proteins, were analyzed by micropipette experiments, but involved membrane proteins reconstituted in artificial lipid membranes [Manneville et al., 1999; Ramaswamy et al., 2000]. None of these methods allows the investigation of transient bending of freely-suspended PM.

1.5.3. Cryogenic high-resolution scanning electron microscopy (Cryo-SEM)

Cryo-SEM is unique in its ability to visualize the ultrastructure of freely-suspended supramolecular assemblies after fast-freezing, freeze-fracture, and sublimation of surface-bound ice. In order to analyze the mechanics of freely-suspended purple membranes cryo-SEM was employed (chapter 3.3. of this thesis) which is increasingly recognized as a powerful tool in material and colloid science [Menger et al., 2002 (1); Menger et al. 2002 (2); Ferrer et al., 2006; Ge et al., 2006].

2. Materials and Methods

2.1. Purple membrane preparation

2.1.1. PM purification

Mutant PM-D96N was kindly provided by Actilor GmbH (Leuna, Germany). Wildtype (PM-WT) and mutant PM-D85T were a gift from Dieter Oesterhelt's group at the Max-Planck Institute of Biochemistry, Martinsried, Germany. All PM preparations were purified by standard procedures [Oesterhelt, Stockenius, 1974]. Briefly, PMs were purified by sucrose-density gradient centrifugation (D(+)-sucrose, biochemical grade, Acros Organics, Geel, Belgium) and washed three times with 1.5 mM phosphate-buffer pH 6.8 (Na_2HPO_4/KH_2PO_4, p.a. grade, Fluka Chemie, Buchs, Switzerland).

2.1.2. PM films

For sugar-embedding of PM 2 mg lyophilized PM were suspended in 100 µl aqueous 25% (w/w) of sugar solution. The solutions were spread onto freshly cleaved mica as well as glass substrates and dried in air. Films of 50-60 µm thickness were obtained. In other experiments matrix-free PM films were prepared directly on mica.

2.2. Spectroscopy

2.2.1. UV-Vis spectroscopy

Temperature-dependent UV spectra were recorded on an Uvikon 922 spectrometer (Kontron Instruments), equipped with a thermostated sample stage. In the case of sugar-embedded PM samples were sealed in cuvettes. Humidity was adjusted by saturated salt solutions.

2.2.2. FT-IR spectroscopy

For FT-IR analyses, PM-sugar films of 5µm thickness were mounted between two CaF_2 windows in order to minimize the influence of residual water. FT-IR spectra were recorded

on a Perkin Elmer FT-IR spectrometer (1600 series), at a resolution of 2 cm^{-1}. Background-corrected spectra were deconvoluted using the program Win-IR Pro (DigiLab).

2.3. Self-assembled monolayers (SAMs) of alkanethiols on gold

2.3.1. Preparation of template stripped gold (TSG)

Template stripped gold (TSG) substrates were prepared by thermal evaporation of gold (~3000 Å) onto the surface of freshly cleaved mica (Plano, Wetzlar) [Wagner et al. 1993]. Glass slides (~1 cm^2) were mounted on top of the gold layer using epoxy glue. After hardening the gold coated glass slides were carefully removed from the mica substrate, and the ultra flat gold surfaces were obtained.

2.3.2. Preparation of alkanethiol SAMs

SAMs of various alkanethiols were prepared on TSG substrates by incubation for 2 h in a 1 mM solution of appropriate polarity (ethanol, n-heptane, deionised water), rinsed with solvent, and dried.

2.3.3. Patterning of SAMs via submerged laser ablation (SLAB)

For submerged laser ablation (SLAB) a pulsed frequency-doubled Nd:YVO_3 laser (Vector 532-100-20, Coherent) and a software controlled galvano scanner system (SCANgine 14®, Scanlab AG, Puchheim; Software: SAM2D, Scaps, Munich) were employed to form structures in the thiol SAMs as well as in the TSG substrate itself (Fig. 6). A focused laser beam (532-nm wavelength, 6 ns pulse length, 20 kHz repetition rate) was scanned over the surface at a speed of 270 μm/s. The total power density was 111 MW/cm^2 for SAM patterning and about 130 MW/cm^2 for gold laser ablation. The beam diameter at focus was determined to be 10 μm. SAM-covered TSG samples were overcoated with a thin layer of a secondary thiol solution. Structures were written in the SAM by pulsed laser ablation. Free TSG structures obtained during laser patterning were refilled immediately with secondary thiol molecules. After 2h the incubation layer was removed. The sample was carefully rinsed with absolute ethanol (water or n-heptane respectively) and overcoated with the next thiol solution (3^{rd} to n-th). The SLAB procedure was repeated. The sample was kept

aligned on stage during the whole patterning procedure. Laser ablation through a covering solution also prevents contamination of the surface with ablated gold particles.

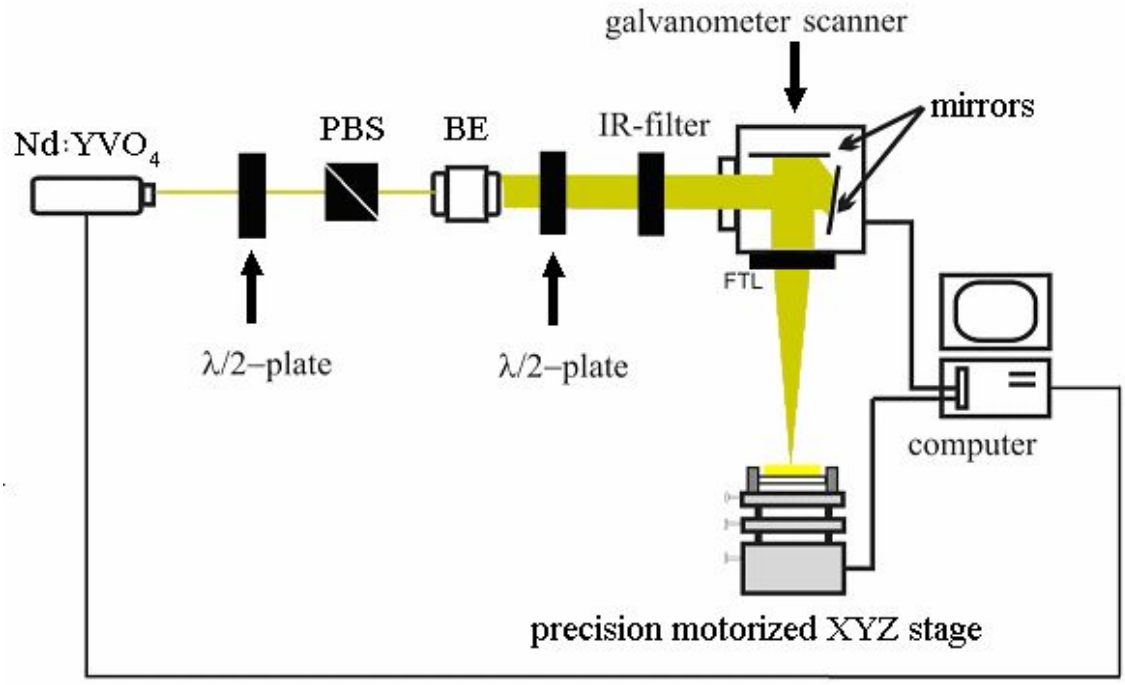

Figure 6 Experimental setup. The beam of a pulsed frequency doubled Nd:YVO_4 was controlled by a galvanometer scanner to form structures in the self-assembled monolayer (SAM) mounted on the precision motorized XYZ stage. Nd:YVO_4 laser, 532 nm, 6 ns pulses, repetition rate 20 kHz. BS: polarizing beam splitter; BE: beam expander; FTL: F-theta lens. IR radiation was blocked by an IR-filter.

2.3.4. Optical microscopy

The result of the patterning procedure was monitored by an optical microscope (Hund, Wetzlar). Different wetting behavior of MHA and DT areas allowed the identification of hydrophilic (MHA) and hydrophobic (DT) areas. Exposure of the surface to water vapor produced contrast sufficient for direct observation and photography of the structured alkanethiol SAMs. The water vapor desorption was retarded by applying a layer of n-heptane.

2.3.5. Cyclic voltammetry

Cyclic voltammetric (CV) analysis of laser-patterned samples was done using a conventional three-electrode system (exposed area 0.5 cm * 1 cm) driven by a computer-controlled model 273A potentiostat (EG&G). Data were obtained using the Model 270 Electro- chemical Analysis Software 3.0 (EG&G). Potentials were measured with respect to a saturated Ag/AgCl reference electrode. As an electrolyte 0.5 mM $K_2[Fe(CN)_6]^{2-}$ and 50 mM KCl in distilled water was used. The cell volume was 20 mL. Scans were started to positive voltages. The scan rate was 50 mVs^{-1}.

2.4. Structural analysis

2.4.1. Atomic force microscopy (AFM)

A variety of alkanethiol SAMs were incubated with PM suspensions (OD ~ 0.3) for 45 min, rinsed with destilled water, and analyzed with a Nanoscope IV AFM (Digital Instruments), operating in tapping mode in air.

2.4.2. Scanning electron microscopy of SAMs

Scanning electron microscopy (SEM) was done with a CamScan (W cathode) or Hitachi (field-emission gun) microscope operating at 15 kV at 20–2000-fold magnification. The current through the samples was about 0.1–0.5 nA.

2.4.3. cryo-SEM of PM

PMs were suspended in 30 mM Tris-buffer, adjusted to different pH values. WT and D96N were analyzed at pH = 9, D85T was analyzed at pH = 7 and 9. Steady-state illumination of PM-WT and PM-D96N was performed with a 100W broadband light-source, leading to a yellow solution in the case of D96N, due to accumulation of M_2-state. 40µl concentrated PM solution (about 10 mg/ml) were placed on the specimen holder of the cryo-transfer system and fast-frozen by plunging it into subcooled liquid nitrogen. In the case of “dark” PM-WT and PM-D96N samples were light adapted first, and fast-frozen under dim light after a delay time of 10 seconds.

Frozen PM specimen were transferred to a nitrogen-cooled preparation unit (Alto 2500, Gatan) via an airlock device, and fractured with a precooled blade to expose a fresh horizontal surface.

The temperature was raised to -95°C for at least 5 min, and surface-bound ice was removed by sublimation. Finally a thin layer of platinum was sputtered onto the sample (10 µA, 60 s) before transferring them into the cryo-SEM (JSM-7500F, JEOL), which was directly coupled to the preparation chamber. Imaging was performed at an acceleration voltage of 1 kV at a stage temperature of -130 °C.

3. Results and Discussion

3.1. Thermochromism of sugar-embedded Purple Membranes

3.1.1. Matrix-dependent thermochromism of BR -The sugar-induced blue membrane (SIBM)

In the following section thermochromic changes of sugar-embedded PMs are described. All PM-sugar samples were used in dark-adapted state for the experiments. Sugars used for the experiments are listed in table 1.

	Disaccharides		Aldohexoses		Ketohexose
Sugars for PM	Trehalose	Sucrose	β-D-mannose	β-D-glucose	β-D-fructose
Structure	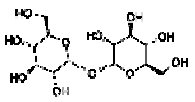	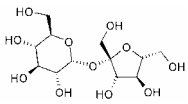	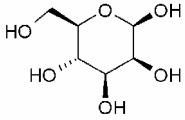	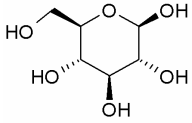	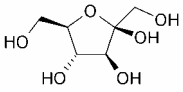
Glass transition*	100	62**	25	31	5

Table 1 Sugars used for SIBM generation. (*) as reported by [Roos, 1993]; (**) rapid crystallization.

Figure 7B shows what is observed when the samples are heated beyond a certain temperature, which is dependent on the carbohydrate species. Shown here is a PM/mannose glass which had its native purple color at room temperature (Fig. 7A). Once heated to 70°C in a dry chamber the color switches from purple to blue. After 2 h of incubation at 70°C the process is completed and no further color change is observed. Upon cooling to room temperature the PM-sugar film preserves its blue color. For other sugars a similar purple-to-blue transition is observed but at varying species-specific temperatures. In order to prove the functionality of BR in these viscous matrices, the light-dark-adapation of the samples was tested. All sugar-embedded PM samples show regular light-dark-adaption (Fig. 7C) but

the kinetics is retarded. This shows that there is enough flexibility in the matrix, at least for BR light-dark-adaption which is accompanied by only minor conformational changes in the bulk protein [Patzelt et al., 2002], and that the protein is functionally active.

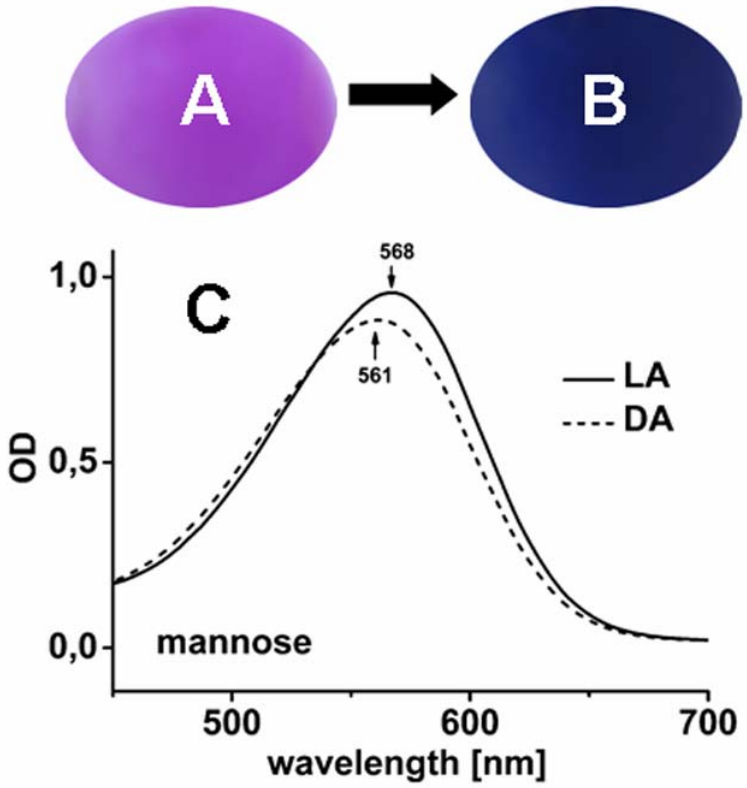

Figure 7 Temperature-induced purple-to-blue transition of purple membranes in a glassy mannose matrix (A) Initial color (B) Color after 2 h incubation at 70°C. The blue color remains when the sample is cooled down to room temperature. (C) Light-Dark-Adaptation of mannose-embedded PM samples at room temperature (LA: light-adapted, DA: dark-adapted). The spectra of glucose- and fructose-embedded PM were essentially the same.

The blue-to-purple back reaction is strongly decelerated and takes several days in dry sugar glasses. However, the regeneration of the purple color proceeds within minutes when the sample is exposed to a 100% humidity atmosphere.

In order to understand SIBM formation in more detail the following questions were experimentally analyzed and a model for SIBM formation was derived.

1.) Preserves sugar entrapment the function of BR?
Is the light-dark-adaption of PM affected by sugar embedding?

2.) Is the SIBM formation depending on the sugar species employed?
Are there structural requirements the matrix molecules need to fulfill?

3.) Is there a threshold temperature for SIBM formation?
Are phase transitions of PM involved?

4.) Is the SIBM formation affected by the availability of divalent cations?
Does cation binding of BR play a role? Are changes observed in the secondary structure of BR?

5.) Is the SIBM formation depending on sample hydration?
Does the reduction of water mechanistically or kinetically influence SIBM formation?

6.) Is SIBM a thermodynamically stable form or is it reverted to PM?
Is there a thermal reversion from SIBM to PM?

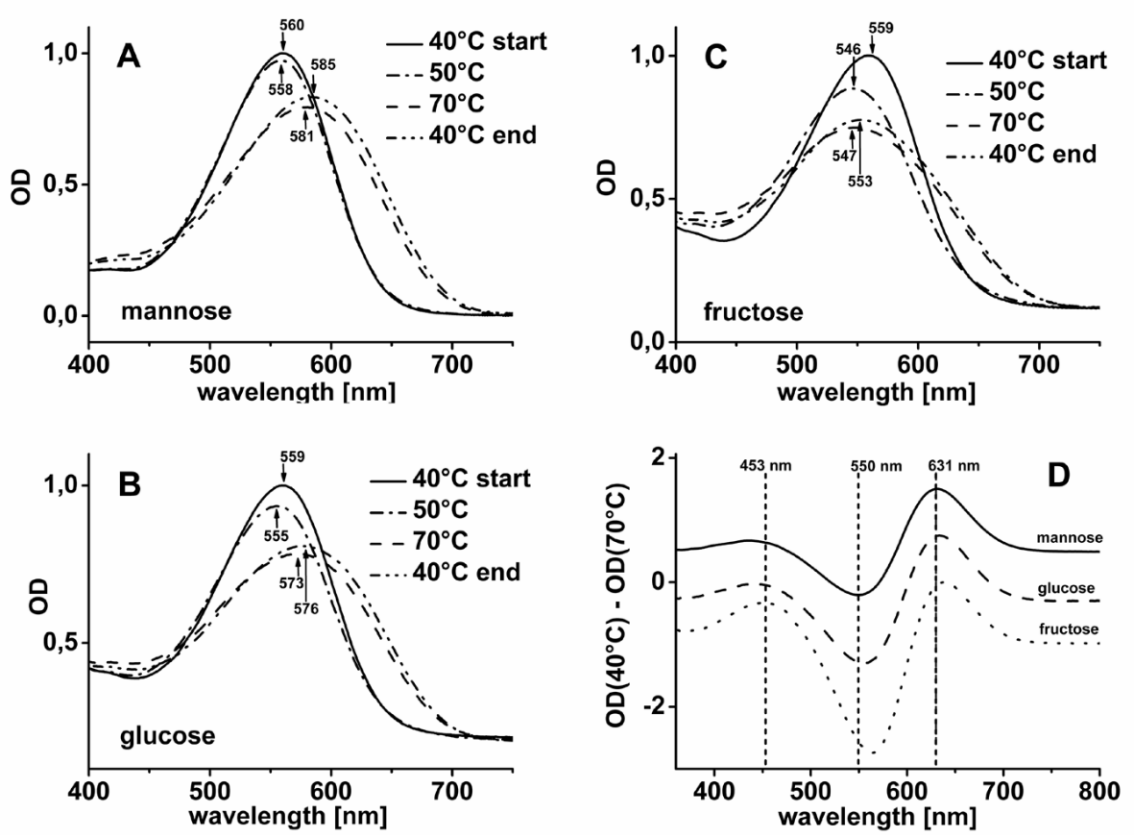

Figure 8 Temperature-dependent spectral changes of various glassy PM-sugar films in the visible. Shown are (A) mannose, (B) glucose, and (C) fructose. In all cases a bathochromic species is formed upon heating the samples to 70°C. After cooling the samples back to 40°C the blue color is still present and will not change for days. (The time course of the SIBM → PM back conversion is discussed later.) (D) Difference spectra of sugar-embedded PM films during SIBM formation (normalized to their bathochromic maxima around 630 nm). The absorption spectra at 40°C served as a reference. Besides the bathochromic state at 630 nm, a hypsochromic species occurs at about 450 nm

Figure 8 shows temperature-dependent absorption spectra in the visible wavelength range of PM, embedded in different sugar matrices. Dark-adapted samples were incubated at various increasing temperatures (40°C, 50°C, and 70°C until steady state was reached), going through the SIBM transition. Then the samples were returned to 40°C, the start value, and measured again.

The absorption spectra document the temperature-induced PM → SIBM transition and proof that species-dependent changes exist. The absorption maxima at 40°C are very close to the values obtained for dark-adapted PM at room temperature. Upon steady-state incubation at 50°C the spectra of all sugar-embedded samples reveal hypsochromic shifts in the order fructose > glucose > mannose (Fig. 8). There are two possible explanations for this observation. It is known that PM undergoes a hypsochromic shift upon extensive dehydration [Renthal et al., 2000]. But if the hypsochromic shifts would be caused by dehydration only then fructose-, mannose- and glucose-embedded samples should show more or less identical hypsochromic shifts because the sugar molecules would bind all water. The observed differentiation matches another line of argumentation, and is most likely based on specific interactions between PM and sugar molecules which are induced or amplified by increasing temperatures. Interaction of PM with a variety of organic compounds (i.e. DMSO) leads to the formation of hypsochromic species which are characterized by absorptions around 460 nm [Oesterhelt et al., 1973; Pande et al. 1989]. Indeed, the difference spectra (Fig. 8D) reveal the rise of a hypsochromic population around 450 nm.

Incubation at 70°C leads to the appearance of states absorbing in the red wing of the spectrum in all sugar-embedded samples, similar to CFBM and ABM formation. At the same time the color of the sugar-derived glasses turns blue (SIBM). A significant bathochromic shift of the visible absorption maxima is observed in the case of mannose- as well as glucose-embedded preparations (Fig. 8A, B). The 70°C spectrum of fructose-embedded samples is considerably broadened (Fig. 8C). However, upon heating hypsochromic populations arise in a sugar-specific amount (Fig. 8), and the spectral maximum of SIBM appears at somewhat shorter wavelength than it is usually observed for suspended blue membranes.

After equilibrating the samples at 40°C again, the SIBM is stable and no noticeable back conversion to PM is observed.

Steady-state incubation at 50°C results in a hypsochromic shift of the absorption maximum in the visible spectra of PM-sugar glasses. No further spectral changes occur from the time on a particular equilibrium value is reached, even if incubation is continued

for a long time. Therefore, visible spectroscopy provides evidence that SIBM formation is suppressed below a certain threshold temperature. This threshold temperature is between 50°C and 70°C.

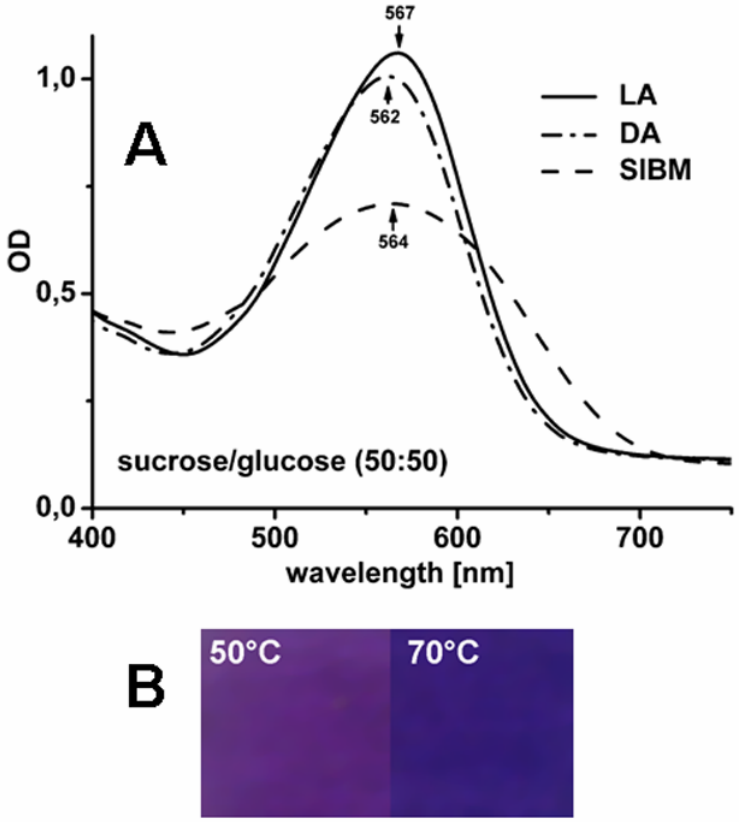

Figure 9 (A) PM in a binary sugar glass. Visible spectra of PM and SIBM, recorded at room temperature. (B) Independence of SIBM formation from hydration changes. A PM-mannose film (~50 µm) was sealed between two glass plates at 50°C, in order to prevent any temperature-induced loss of water. Incubation at 70°C leads to SIBM formation wherefrom is concluded that SIBM formation is not coupled to water removal from the sample.

Pure sucrose-derived glasses show rapid crystallization. This obstacle was overcome by the preparation of a 50:50 (w/w) sucrose/glucose binary glass (glass transition: 47°C) [Orford et al., 1990]. Figure 9A shows the visible absorption spectra of sucrose/glucose-embedded PM before and after SIBM formation. With respect to the hypsochromic species formed at wavelengths less than 500 nm and the absorption maximum, the sucrose/glucose SIBM spectrum resembles a superposition of those spectra obtained with glucose- and

fructose-embedded samples. As sucrose consists of glucose and fructose monomers, it is reasonable that the properties of sucrose resemble those from its building blocks.

With trehalose-embedded samples SIBM formation is not observed. From a chemical point of view trehalose is similar to sucrose as both are disaccharides. But since trehalose has a rather high glass temperature of about 100°C [Roos, 1993] this proves that the phase state of the sugar matrix (glass/rubber) is an important parameter for SIBM formation.

3.1.2. The role of water and divalent cations

The steady-state incubation at various temperatures below the threshold value of a particular sample causes specific changes, but do not lead to SIBM formation. The visible spectroscopy results were complemented by photographic detection of color changes that go along with distinct steps of the SIBM formation and PM regeneration.

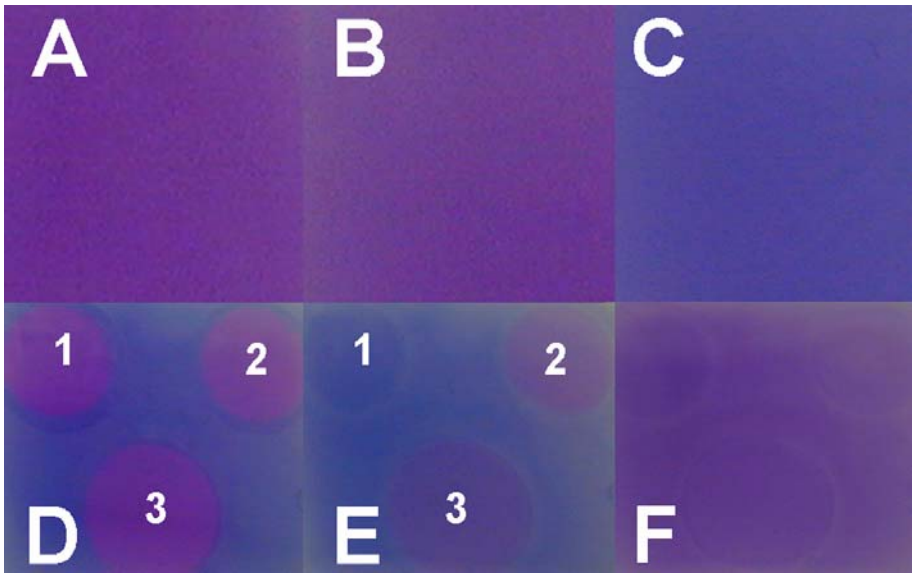

Figure 10 Influence of incubation time and cations on SIBM formation. (A) Image of a mannose-embedded PM film (~50 µm) on an isothermal heating plate at 50°C. (B) The same film after 24 h incubation. The native purple color is unchanged. (C) Incubation at 70°C results in SIBM formation. (D) Regeneration of PM subsequent to treatment with (1) water, (2) 50 mM $MgCl_2$ and (3) 50 mM $CaCl_2$. (E) Incubation at 70°C. SIBM formation is suppressed by $MgCl_2$ (spot 2) and $CaCl_2$ (spot 3). (F) At room temperature the sample is reverted to purple in a viscosity-dependent manner.

Figure 10 demonstrates the influence of incubation time and cations. A PM-mannose film is incubated at 35°C on an isothermal heating plate for 3 days, and subsequently equilibrated at 50°C (Fig. 10A). Upon 24 h incubation at 50°C, the native purple color does not change (Fig. 10B). Once the incubation temperature is switched to 70°C, SIBM formation takes place. The color turns from purple to blue, and the conversion is completed after 1 h (Fig. 10C). The timescales indicate contributions from a thermodynamical (phase-transition-like) barrier related to SIBM formation, rather than for a kinetic effect, as 24 h incubation at 50°C do not result in any SIBM formation, while at 70°C the conversion starts immediately, and the process is completed within 1 h.

The sample is cooled down to 25°C, and treated with 1 µl drops of H_2O (spot 1), 50mM $MgCl_2$ (spot 2) and 50mM $CaCl_2$ (spot 3). SIBM is reverted to PM selectively in the locations where the drops were placed (Fig. 10D). After 24 h of incubation at 70°C, SIBM is recovered at the location where the drop of pure water was placed (spot 1), but Mg^{2+} and Ca^{2+} inhibit SIBM formation effectively (Fig. 10E). At 25°C SIBM converts back to PM within 24 h at a relative humidity of 50% (Fig. 10F). Water is considered to mediate the viscosity of the samples. As was shown by the visual spectroscopy experiments, preparation of dry PM-sugar films is not sufficient to induce the purple-to-blue transition of embedded PM. Thus the SIBM phenomenon is not a dehydration effect. This interpretation is supported by the fact that SIBM formation occurs also in sugar-derived glasses which where sealed prior to incubating at 70°C (10B).

The properties of sugar glasses depend on their water content. The glass transition temperature as well as the viscosity decrease with increasing water content [Roos, 1993]. Application of water leads to a decrease in viscosity. As a result, the SIBM→PM conversion is speeded up, which is otherwise kinetically slowed down by the viscous matrix.

3.1.3. Model for SIBM

An insight into the nature of SIBM comes from the influence of cations on SIBM formation. As shown in Figure 10E, an excess of divalent cations in the sugar glass is able to inhibit SIBM formation. Therefore, it is reasonable to conclude that SIBM formation is based on reversible cation removal in a similar manner as it is the case in cation-free blue membrane (CFBM).

It is known that earth alkaline metal ions form complexes with carbohydrates [Angyal, 1981; Whitfield et al., 1993]. Beyond the physico-chemical aspect, metal complexation by carbohydrates plays an important role in structural biology and molecular medicine. A prominent example is the class of mannose binding proteins (MBP) which are involved in cell-cell interaction and immuno-defense [Sheriff et al., 1994; Thompson, 1995; Drickamer, 1999]. At the carbohydrate recognition domain of MBPs a Ca^{2+} ion is directly co-ordinated to two hydroxyl groups of mannose [Weis et al., 1992; Harte et al. 1994; Liang et al. 1996].

The initial research focused on metal-carbohydrate interactions in aqueous solution where metal binding to carbohydrates is very weak, because sugar molecules cannot compete effectively with the water molecules for metal complexation [Angyal, 1981; Angyal, 1989]. In that case, the prerequisite for optimal sugar-cation complexation is a sequence of axial, equatorial, axial -OH groups (a-e-a), and only a limited set of carbohydrate-metal complexes is observed [Angyal, 1981]. In contrast to this, strong carbohydrate-cation complexes are readily formed in the absence of free water [Puzo et al., 1985; Lemoine et al., 1991; Hofmeister et al., 1991; Fura, Leary, 1993]

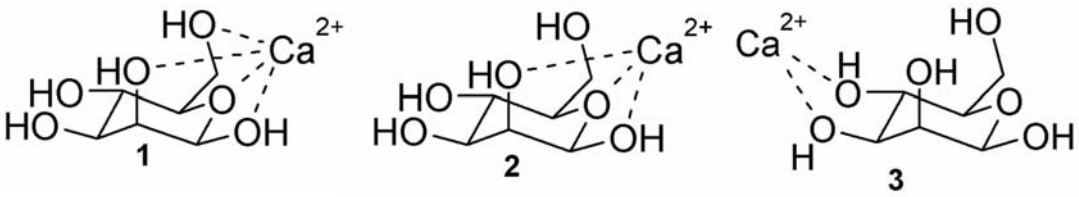

Figure 11. Complex formation between calcium and mannose via oxygen atoms [Wong et al., 2001]. (1) tetradentate mode; (2) tridentate mode; (3) bidentate mode.

Density functional theory (DFT) has been used to analyze the structural determinants of metal binding by carbohydrates [Zheng et al., 1997; Wong et al., 2001]. In the case of β-D-mannose several stable mannose-Ca^{2+} complexes were identified, and the corresponding energies and bond lengths were calculated [Wong et al., 2001]. Three classes of mannose-Ca^{2+} complexes were revealed (Fig. 11). The most stable binding mode is the tetradentate mode, followed by the tridentate, and bidentate mode.

At this point, some comments on the nature of sugar glasses are worthy. Carbohydrates are natural glass formers. Once amorphized, they may exist as solid "glasses" or liquid-like "rubbers" [Roos, 1993]. The transition between these two states is commonly known as "glass transition" and is characterized by the glass transition temperature T_g. Above the glass transition temperature the viscosity decreases considerably. The sugar molecules acquire a somewhat higher mobility and are thus able to facilitate the diffusion of cations in the matrix. To generate SIBM, the sugar matrix glass therefore ought to be in the rubber-like state. Once released from PM, divalent cations diffuse on a potential surface which is comprised of many shallow energy minima, provided by the amorphous network of chelating sugar molecules.

However, a difference between SIBM formation and the preparation of CFBM is evident. Since a particular threshold temperature exists, independent of sugar transitions, it is concluded that temperature-dependent changes in the secondary structure of PM must occur which weaken the PM-cation bonds. Once weakened, carbohydrates replace the native cation binding sites in PM.

The need for structural transitions in PM upon SIBM formation provides indirect evidence for the existence of specific cation binding sites in PM. Because, given that at 50°C all sugars used are in the fluid ("rubber-like") state above their glass transition temperature, unspecifically attached, and therefore loosely bound cations would be immediately released into the chelating sugar matrix.

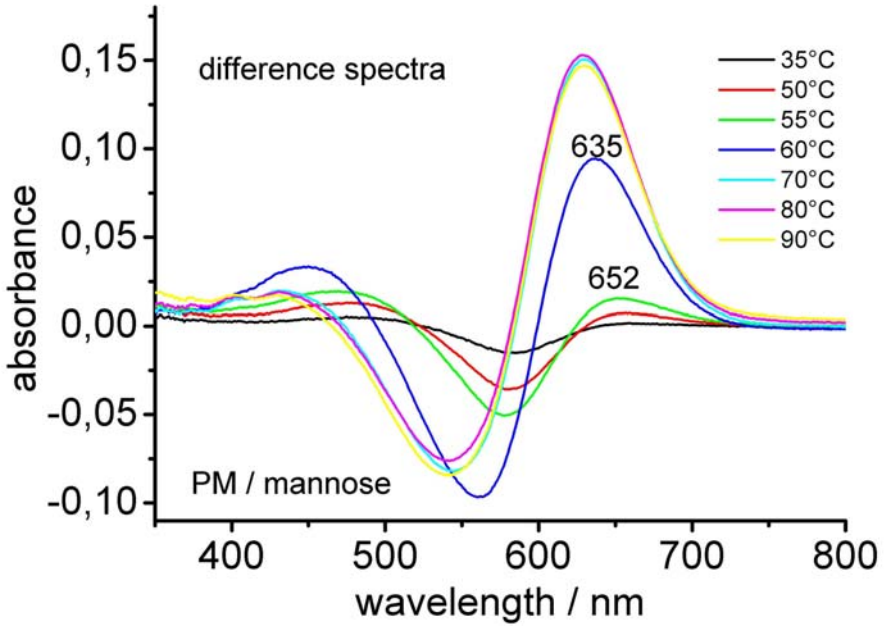

Figure 12 Temperature-dependent UV-Vis difference spectra of mannose-embedded PM (reference: 20°C). The PM→SIBM transition is observed upon steady-state incubation at 60°C. Increasing the temperature to 70°C leads to an increase in intensity and is accompanied by further spectral contributions to the bathochromic part of the spectrum.

Upon heating PM undergoes several phase transitions which involve changes in BR secondary structure and trimer assembly [Jackson, Sturtevant, 1978; Brouillette et al., 1987; Cladera et al., 1988; Arrondo et al., 1994; Taneva et al., 1995; Heyes, El-Sayed, 2001; Sonoyama, Mitaku, 2004]. Additionally, it has been observed that above 70°C blue membrane preparations poorly bind cations, indicating that the conformation of the binding site has changed [Chang et al., 1986].

Fig. 12 shows temperature-dependent difference spectra which prove that the PM→SIBM occurs from the time when the incubation temperature is raised to 60°C. Upon steady-state incubation at 70°C the bathochromic portion of the spectra increases which indicates that more than one phase transition might contribute to SIBM formation due to the combination. Furthermore, it is known that the retinal isomeric composition of dark-adapted BR is shifted to all-trans sharply at temperatures about 70°C [Druckmann et al., 1982] which would lead to an increase in spectral intensity due to the higher extinction coefficient of all-trans retinal.

Following the EPR experiments mentioned above [Eliash et al., 2000], the B-C loop, together with a glycolipid molecule, would comprise a high-affinity binding site, which is disordered in blue membrane [Okumura et al., 2005]. From the time when the conformational change at the cation binding site has taken place, i.e. the β-structure of the B-C loop has disappeared, the cations are able to leave PM, and are entropically diluted in the sugar glass. Upon cooling, the viscosity of the dry sugar matrix increases considerably, decelerates the reassembly of the binding site, and traps the cations in a metastable state.

The model presented above is supported by observations made with the blue mutant PM-D85T which has a bathochromically shifted spectrum compared to PM-WT. Mannose-embedded PM shows thermochromic changes inverse to those observed with PM-WT [Fig. 13]. Upon cation removal by EDTA treatment PM-D85T suspensions experience a hypsochromic shift of 15 nm, and the color changes to purple.

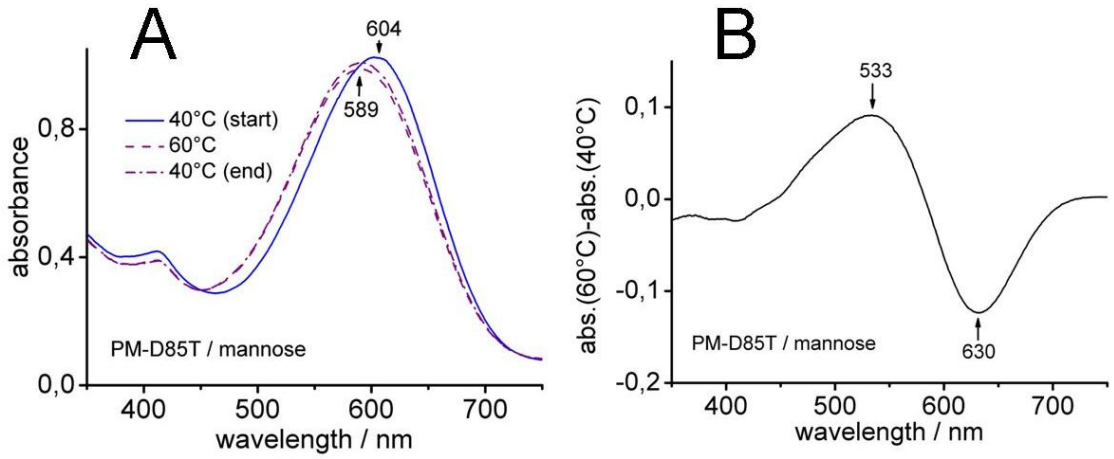

Figure 13 Temperature-dependent changes of mannose-embedded PM-D85T. (A) UV-Vis spectrum of PM-D85T before and after going through the 60°C transition. (B) Difference spectrum according to decay of the bathochromic population due to "sugar-induced purple membrane" formation by PM-D85T.

Therefore, it is reasonable that conformational changes which lead to SIBM formation in the case of PM-WT result in formation of "sugar-induced purple membrane" in the case of PM-D85T. Furthermore, this is an indication for similar ways of cation binding in PM-WT and PM-D85T.

3.1.4. Thermal reconversion of SIBM to PM monitored by visible spectroscopy

A mannose-embedded SIBM sample was placed in a spectrometer (40°C, steady-state), and time-dependent visible spectra were collected. The visible spectra do not show any significant changes during the first 90 h (Fig. 14A).

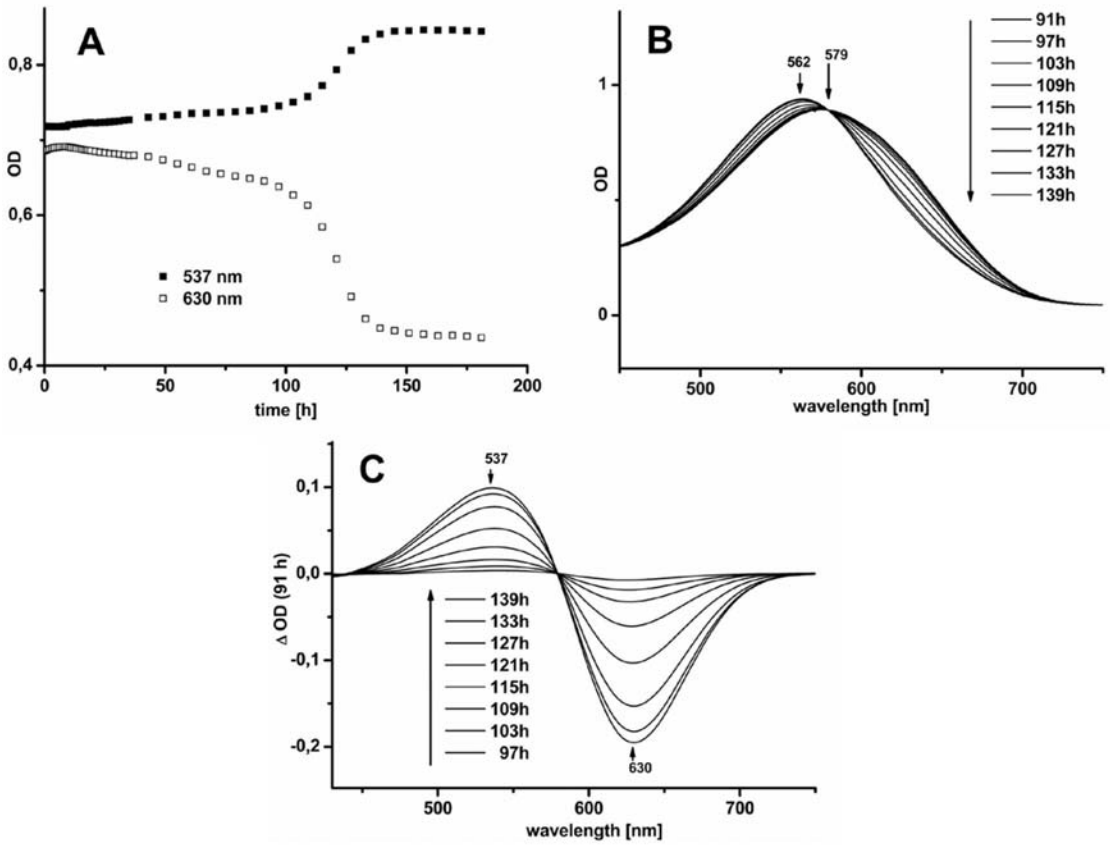

Figure 14. Kinetics of the re-conversion of SIBM to PM in a mannose film. (A) Time dependence of SIBM to PM conversion at 40°C monitored by the spectral changes occuring at 537 nm (filled squares) and 630 nm (empty squares). (B) The blue-to-purple re-conversion of SIBM to PM. Time-dependent visible spectra of SIBM in a mannose film starting with the spectrum at 91 h. (C) Time-dependent difference spectra in the visible of the SIBM to PM transition. The difference spectra refer to the absorption spectrum taken at 91 h as a reference.

After ~100h the SIBM to PM conversion starts rapidly and is completed within 20 h. Figure 14B shows a sequence of time-dependent spectra, beginning with the visible spectrum recorded 91 h after steady-state incubation of SIBM. In Figure 14C, the corresponding time-dependent difference spectra are shown, with the 91 h spectrum as reference. The existence of an isosbestic point at 579 nm strongly indicates the interconversion of two species which absorb at 630 nm and 537 nm, respectively. In Figure 14A the time-dependent development of amplitudes corresponding to these species is illustrated. The curves support the hypothesis of a phase-transition which alters the cation binding capability of PM. This phase transition is decelerated by the sugar matrix. As soon as the phase transition is completed PM recovers its cation binding ability and is back-titrated to the purple form from the surrounding cations. This finding signals that a phase transition of PM triggers the interconversion of blue to purple.

3.1.5. Differences in secondary structure of PM and SIBM

The top lines in Fig. 15 show deconvoluted FTIR spectra of sugar-embedded PM. All sugar-embedded samples show the amide-I band centered around 1664 cm^{-1}. This signal resembles the well-known mixture of α_I- and α_{II}-helices, with the α_{II}-helical content giving rise to a signal at 1665 cm^{-1}. Upon SIBM formation the α-helical spectral region keeps almost unchanged. In all samples some loss of intensity in the region between 1620 and 1640 cm^{-1} is observed, usually assigned to β-sheet [Cladera et al., 1992]. Additionally, the signal decreases between 1670 and 1690 cm^{-1}, indicating a loss of β-turns. A disordered β-structure would resemble the observations made with the current x-ray structure of blue membrane [Okumura et al., 2005]. The FTIR spectra give evidence for the retention of α_{II}-helices in sugar-embedded PM. Thus sugar-embedding cannot count for the notorious invisibility of α_{II}-helices in electron microscopic studies of PM. [Grigorieff et al., 1996, Kimura et al., 1997].

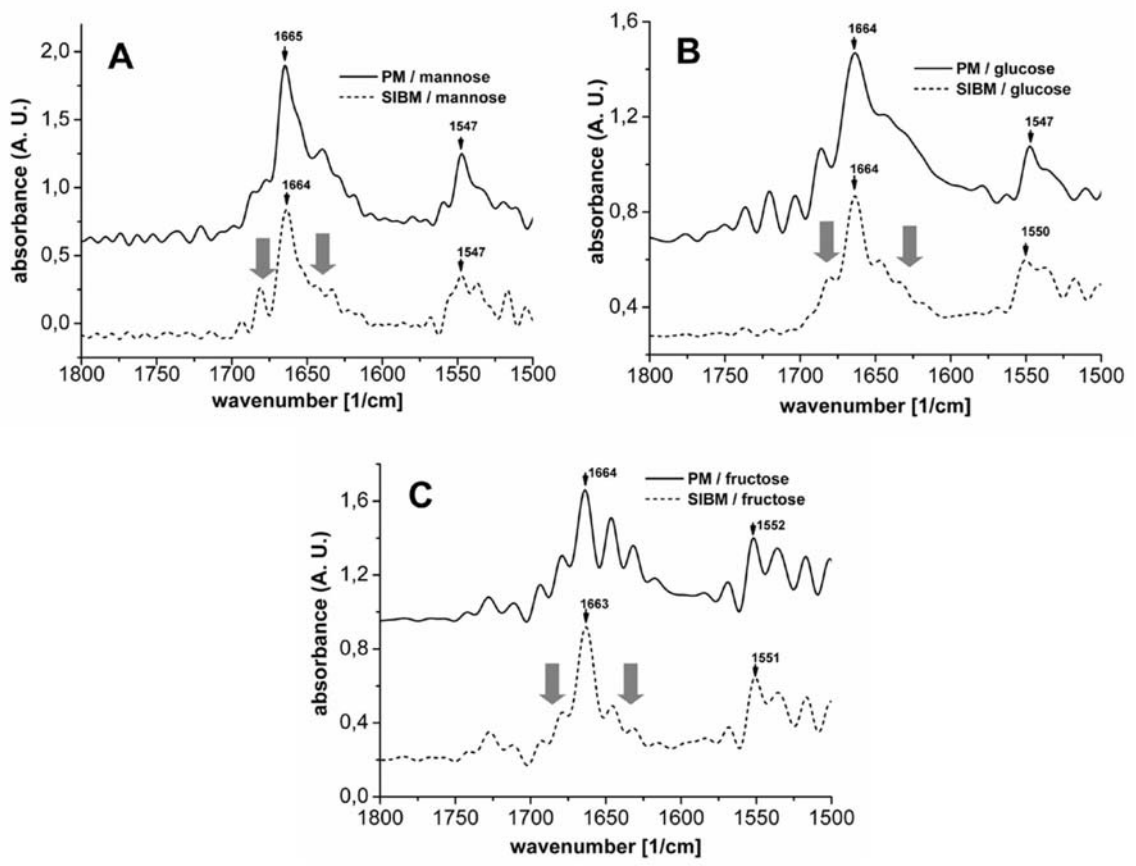

Figure 15 FTIR-analysis of sugar-embedded PM samples. (A) mannose; (B) glucose; (C) fructose. Decrease in β-structure is marked by grey arrows.

3.2. Solid-supported assembly of purple membranes

3.2.1. Thermochromism of solid-supported PM

Beyond the matrix-dependent spectral changes due to SIBM formation, which were discussed in section 3.1., the temperature-dependent difference spectra (Fig. 12) reveal further thermochromic changes at 460 nm and 650 nm, however, with smaller intensities. To distinguish between the different kinds of spectral changes matrix-free films of PM-WT were prepared on mica, and thermochromic changes were observed at different humidities.

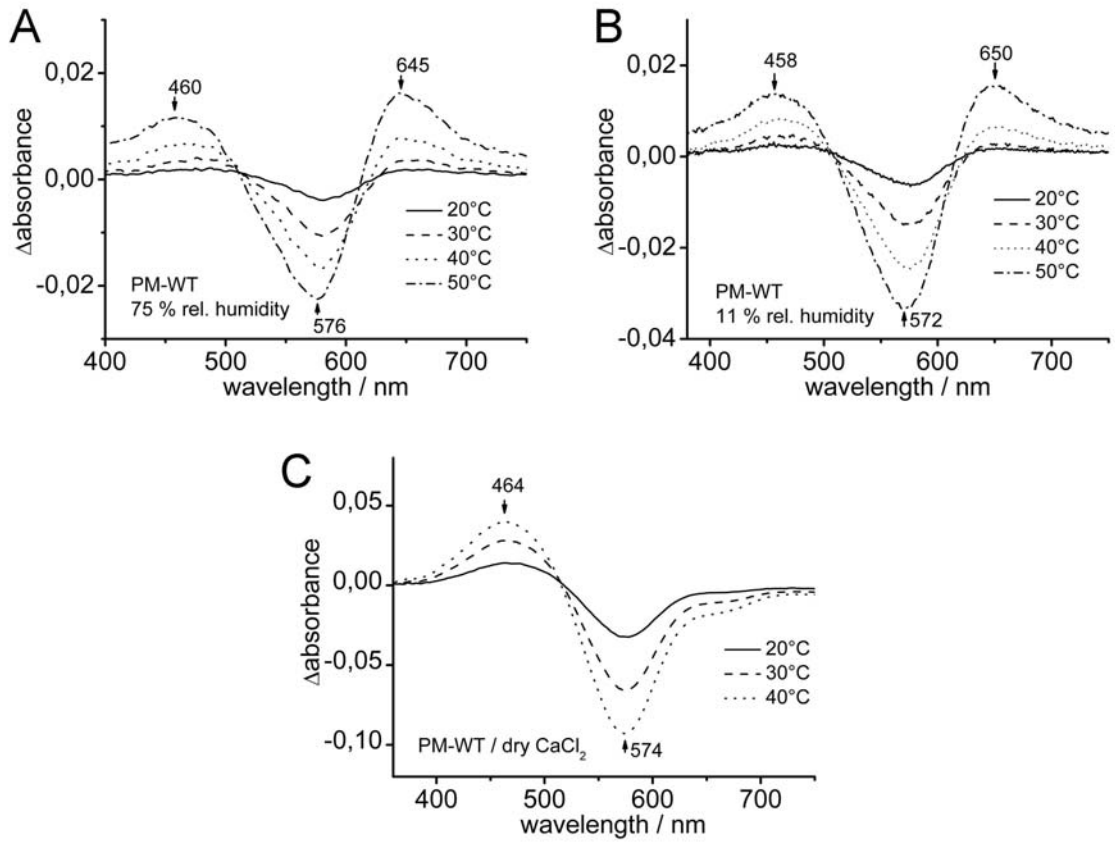

Figure 16 Thermochromic changes of solid-supported PM and its humidity dependence. A Film of PM-WT on mica at 75 % humidity. B Film of PM-WT on mica at 11 % humidity. C Film of PM-WT on mica above $CaCl_2$.

Indeed, spectral states at 460 nm as well as 650 nm emerge when PM films on mica are incubated at humidities down to 11 % (Fig. 16). The 460 nm state resembles the so called type-I-thermochromism [Neebe et al., 2008] and is due to Schiff base deprotonation. As

mentioned in section 3.1.1. this state is also observed when the BR framework is weakened by interaction with organic solvents [Oesterhelt et al., 1973; Pande et al. 1989]. The 650 nm state has been observed previously, and is not due to the formation of common "blue membrane" [Neebe et al., 2008]. Although its exact nature is unknown, in another context it has been assigned to temperature-dependent equilibria between the B- and O-state of BR [Shen et al., 1993] Interestingly, the bathochromic population is not observed under harsh dehydration conditions, using $CaCl_2$ as desiccant, while the 460 nm state is still present (Fig. 16C). It is concluded that the bathochromic state is no longer thermally accessible at low hydration conditions. This is in line with previous studies which indicated that upon dehydration the O-state is no longer observed in the photocycle [Korenstein, Hess, 1977; Fitter et al., 1996; Ganea et al., 1997]. This reflects the importance of water residues for the function of BR which has emerged from a variety of structural and spectroscopic studies [Luecke, 2000; Kandori, 2000]. From a technological point of view, the solidity of type-I-thermochromism, even under harsh dehydration conditions, is an interesting feature which could be used in a variety of applications including security tags.

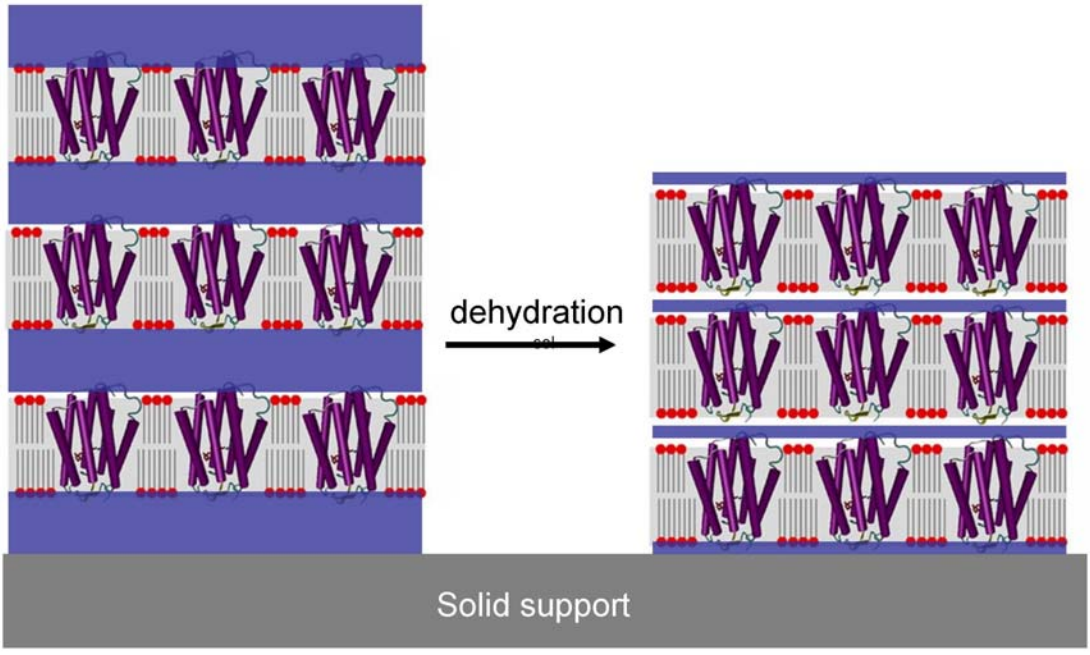

Figure 17 Hydration dependence of PM-PM distance in solid-supported PM films. At low hydration levels PM-PM interactions become dominant.

Furthermore, the distance between single PM sheets in solid-supported films is a direct function of hydration [Salditt et al., 1999]. As the hydration level decreases the interaction forces between PM layers increase significantly (Fig. 17). These inter-membrane interactions possibly will put constraints to the conformational flexibility of BR which in turn will alter its functionality.

3.2.2. Adsorption of PM on SAMs

Because of its size PM patches do not show significant diffusion, and adsorption-based methods are the only way for the immobilization of PM on surfaces. The immobilization of negatively charged membrane protein complexes to the surface of alkanethiol SAMs comprising cationic end groups has been demonstrated earlier [Valiokas et al., 2006]. In this study patterns of positively charged alkanethiols were written into protein repelling [Harder et al., 1998] polyethylene glycol (PEG) SAMs. The surface of PM is negatively charged thus making this approach a promising method for the surface immobilization of PM (Fig. 18). In difference to single membrane protein complexes, PM comprises thousands of BR molecules organized in a micronsized 2-D crystal. At first, the applicability of SAM-based adsorption must be proved. But the fabrication of micron sized alkanethiol patterns which are suitable for PM adsorption remains the biggest challenge and will be the discussed in the next chapter.

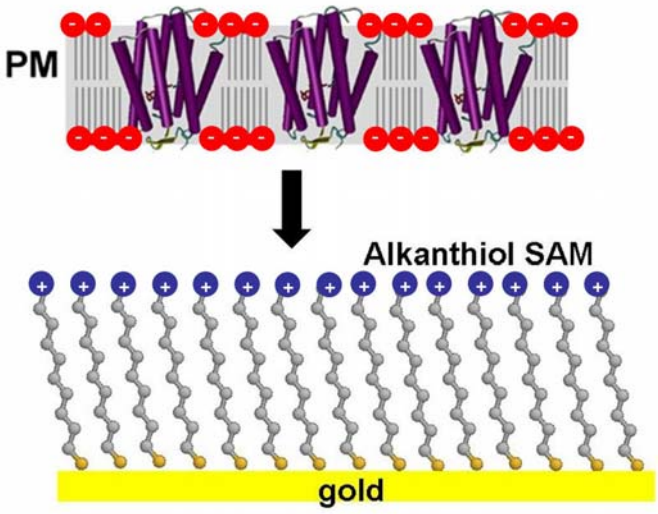

Figure 18 Immobilization of PM on positively charged SAMs. Adsorption is primarily mediated via negatively charged lipid head groups.

The applicability of the adsorption-based approach for the surface immobilization of PM was demonstrated in two ways. The first approach followed the method of Valiokas et al. and employed positively charged aminoethanethiol (AET) SAMs as well as PEG-SAMs on ultrasmooth gold surfaces. The second approach made use of negatively charged SAMs of mercaptoundecanoic acid (MUA), and was inspired by the common procedure for electrostatically balanced AFM imaging of PM on mica [Müller et. al., 1999 (2)].

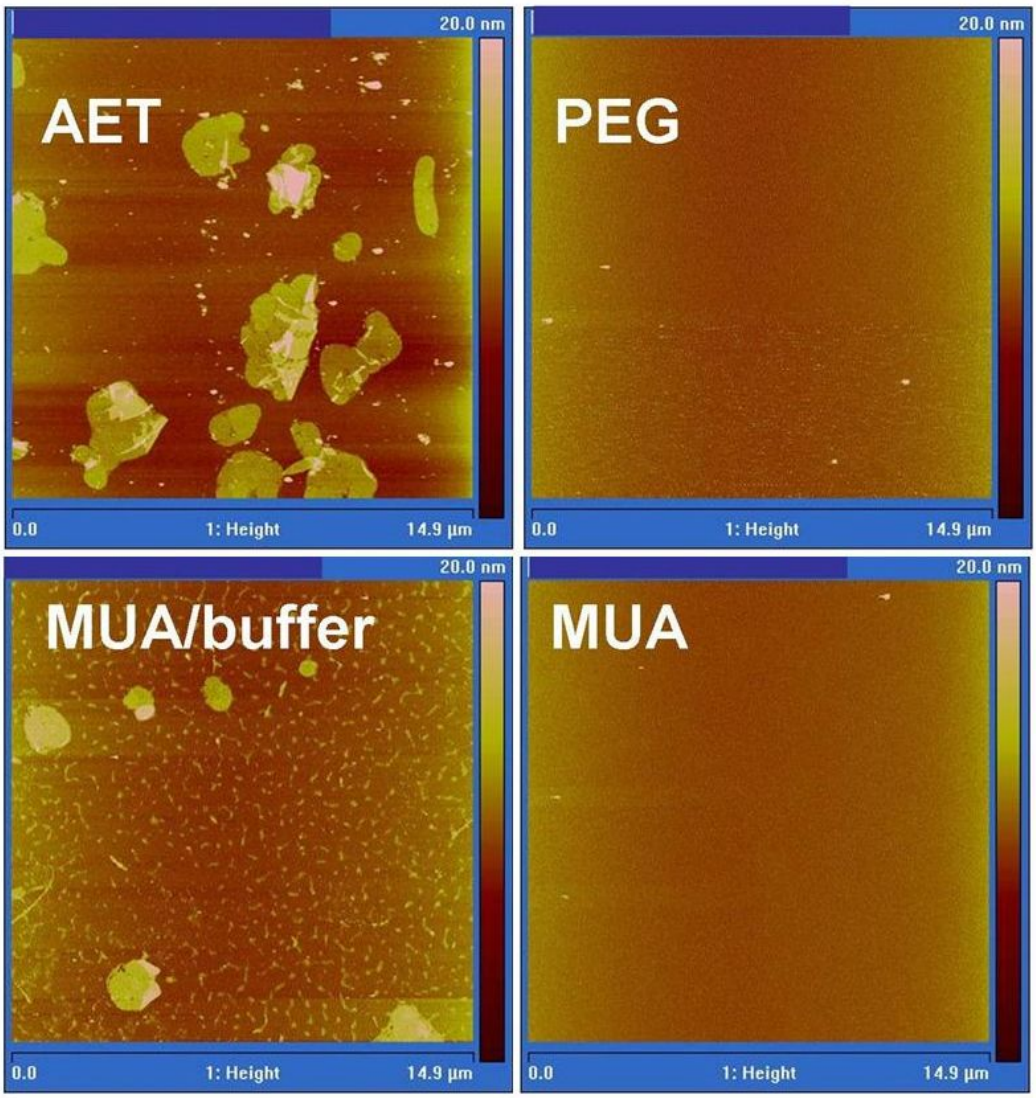

Figure 19 AFM images of SAMs after incubation with PM (OD = 0.3, t = 45 min). Cationic: AET; Anionic: MUA; Neutral and protein repelling: PEG. In the case of MUA/buffer the incubation suspension was buffered by 300 mM KCl / 10 mM Tris-pH 9.

AFM images were taken at various locations on the TSG samples to get statistically-interpretable results.

Figure 19 shows representative AFM images of alkanethiol-covered TSG samples incubated with PM. As expected PM adsorbed readily on positively charged AET-SAMs, and no PMs were found on PEG- SAMs in any case (Fig. 19, top).

Around pH = 7 MUA-SAMs are negatively charged which leads to repulsive interactions with negatively charged PMs. Therefore, PMs did not adsorb to bare MUA-SAMs. When buffered by 300 mM KCl / pH = 7.8 membrane patches adsorbed well to the surface (Fig. 19, bottom). The negative charge is effectively shielded due to the high salinity of the buffer.

This demonstrates that the method of SAM-based adsorption of membrane protein complexes [Valiakos et al., 2006] is applicable for the immobilization of micron sized PMs.

To achieve spatio-selective immobilization of PMs on distinct locations on a biochip SAMs have to be structured at the micron scale. In the next chapter a procedure is presented which enables the high-throughput fabrication of structured SAMs comprising lateral dimensions up to several hundred micrometers.

3.2.3. Fabrication of structured self-assembled monolayers of alkanethiols

3.2.3.1. Submerged laser ablation (SLAB) – The process

Submerged laser ablation (SLAB) enables the preparation of complex patterned SAMs, free gold areas suitable as electrodes and in addition laser patterning of the substrate itself in a single process. (Fig. 20) A template stripped gold (TSG) substrate, mounted onto a glass carrier by epoxy glue, is covered with a self-assembled monolayer (SAM) of a first thiol (primary thiol). The assembly is then submerged into a solution of a second thiolated compound (secondary thiol or reactant). The laser beam incidents to the TSG passing through the reactant solution and the SAM formed by the first thiol.

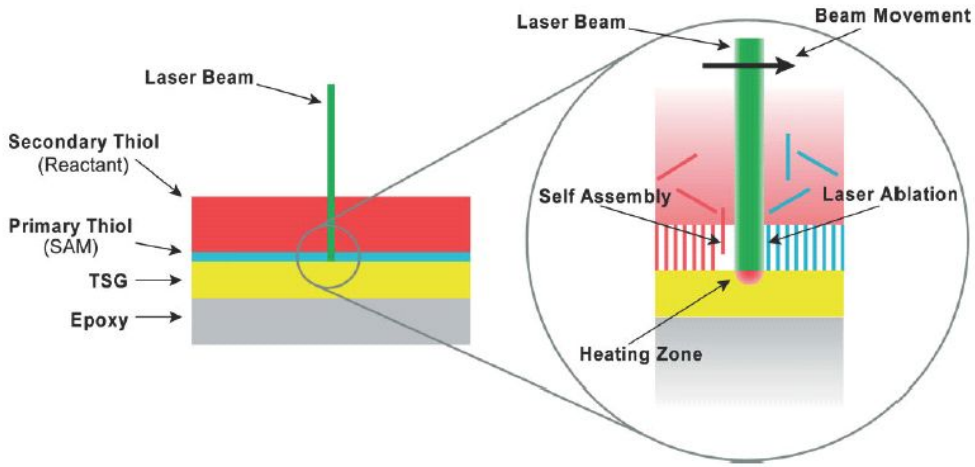

Figure 20 Illustration of the submerged laser ablation (SLAB) process. Left: Template-stripped gold (TSG) substrate covered by a self-assembled monolayer (SAM) of the first thiol (primary thiol) with a layer of a second thiolated compound (secondary thiol or reactant) on top. Right: The gold area where the laser beam hits the surface is heated and the sulfur–gold bond is thermally cleaved. Scanning the laser beam leads to a dynamic process, in which the primary thiol is ablated and replaced by the secondary thiol from the liquid phase.

The gold area where the laser beam hits the surface is heated due to the partial absorption of the laser light. The intensity is chosen low enough not to cause any ablation process in the TSG layer itself, but high enough to thermally split the sulphur-gold-bond which binds the primary thiol to the TSG substrate. In the direction of the laser beam movement the primary thiol is released from the surface. As soon as the laser beam proceeds, the surface temperature decreases and secondary thiol fills in from the supernatant forming covalent

bonds with the TSG. In all cases where the reactant tends to self-assemble an electrically insulating densely packed SAM is obtained, which contains a monomolecular structure of the reactant embedded into the primary thiol. This process can be repeated numerous times with the substrate in place, leading to complex patterned monolayer structures. Electrical contacts of bare gold are obtained when no reactant is in the overlayer during the SLAB process.

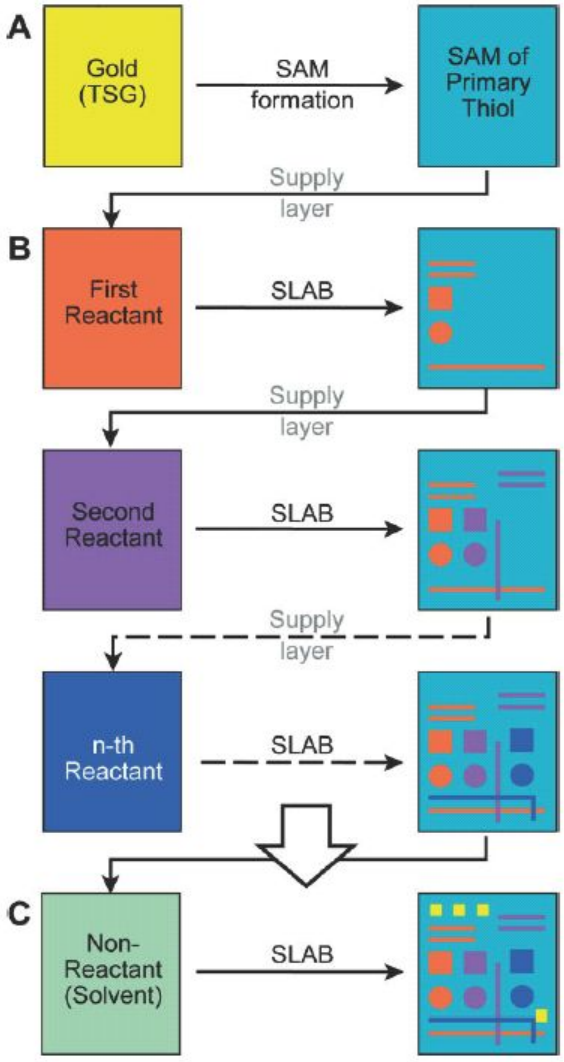

Figure 21 Preparation of multicomponent patterned monolayers. A) SAM of primary thiol formed on gold. B) The reactant solutions (2^{nd} to n-th step) cover the whole surface of the substrate. During SLAB, the reactants replace thiols previously bound to the substrate. C) Optional bare-gold contacts can also be prepared, for example, for contacting with electronics.

The SLAB process comprises three key steps (Fig. 21): First on the gold substrate a self-assembled monolayer (SAM) of the primary thiol is formed. Secondly the first reactant is supplied as a solution covering the whole surface of the substrate. At the positions where SLAB is done the first thiol is replaced by the reactant from the supernatant. The gold linkage of the primary thiol is cleaved and the primary thiol is removed from the gold. With a pulse energy of about 110 MW/cm^2 no damage is caused to the gold substrate itself, but the thiol bond is cleaved and the bound thiols are released. The thiol in the supernatant (reactant) assembles on the bare gold from the solution due to Brownian diffusion. A careful setting and control of the pulse intensities is required to obtain a highly selective ablation of the monolayers without causing any ablation of the supporting gold layer.

This process may be repeated with further reactants as often as required. Numerous consecutive ablation steps can be done without removing and repositioning the substrate. Therefore realignment of structures is not an issue. Wherever SLAB is applied all molecules assembled earlier are removed and only the last species supplied will be in the laser exposed areas. This allows the preparation of surfaces fully covered by a monomolecular layer consisting of numerous well-defined different molecular species. Diffusion of alkanethiols into bare regions is a problem in some chemical patterning schemes. Microdisplacement printing was suggested to diminish diffusion during microcontact printing [Dameron et al., 2005]. It is one of the advantages of SLAB that bare gold areas are covered immediately by the second alkanethiol from the supernatant during the laser-controlled exchange process and for this reason diffusion is immediately hindered.

3.2.3.2. Analysis by scanning electron microscopy (SEM)

The analysis of the SLAB process was accomplished by scanning electron microscopy (SEM). SAMs produce different SEM contrast according to variations in end group, chain length and conformational order [López et al., 1993].

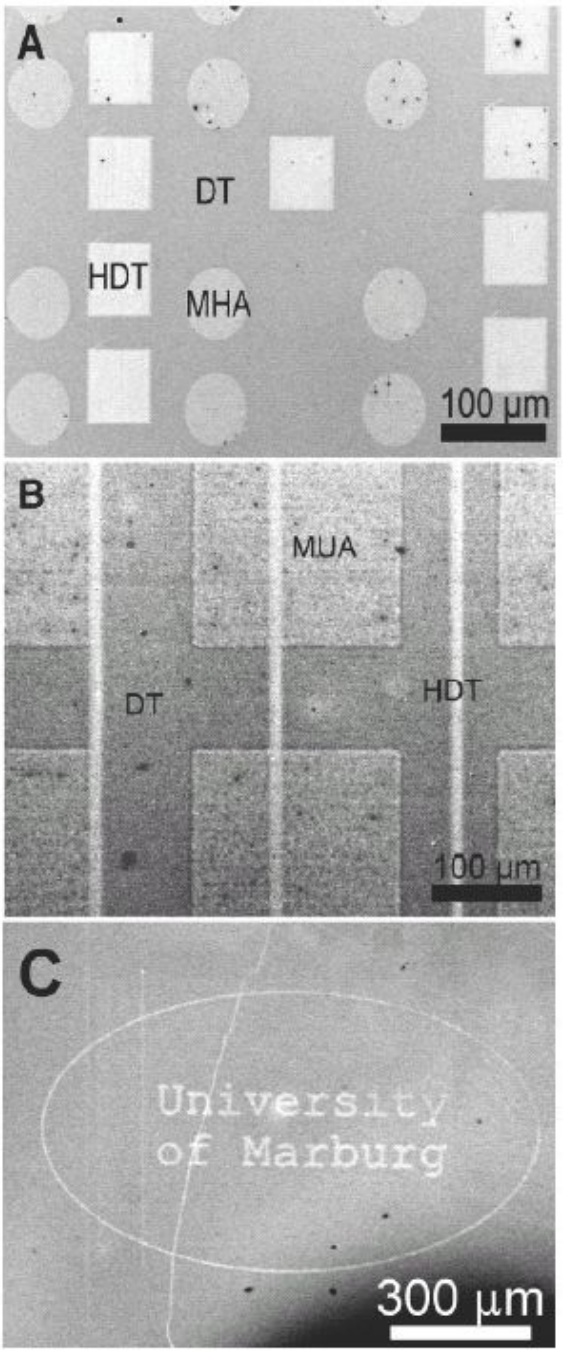

Figure 22 SEM images of multicomponent patterned SAMs. A) A patterned DT SAM, on which in subsequent steps circles of MHA and squares of HDT were prepared by SLAB. The black spots are damage in the SAM caused by the electron beam. B) Demonstration of the first-in first-out principle. An array of MUA squares was first generated in a SAM of DT, and in a second step parallel lines of HDT were prepared. During this second SLAB process all earlier SAMs were removed and replaced by HDT. C) In a dithiothreitol (DTT) SAM, a logo was created by SLAB. The letters and the line are bare gold, as might be required, for example, for electrical contacts.

In Figure 22 SEM images of structured alkanethiol monolayers are shown. Fig. 22A demonstrates that in subsequent steps a primary thiol SAM made from DT was patterned by SLAB first with MHA (circles) and then with HDT (squares). Neither the DT monolayer nor the MHA circles were affected by the preparation of the HDT squares. This demonstrates that the reaction is strictly limited to the laser exposed area. Overlapping structures are shown in Fig.22B. First a micro array of MUA squares was created in the primary DT SAM by SLAB. In the next step this micro array was overwritten by parallel HDT lines. This experiment shows that any earlier structuring process will be erased by a later one. The preparation of the HDT lines causes that the DT monolayer as well as the MUA monolayer are both removed and replaced by HDT. This is seen best at the transitions between DT and MUA. Finally it is possible to generate gold contacts by SLAB of a monolayer without replacing the released thiol by another species. This is shown in Fig. 22C where a short logo was generated by laser ablation.

Submerged laser ablation (SLAB) allows the structuring of monolayers. It was observed that gold laser ablation in air causes the generation of numerous micronsized particles, which damage the monolayers due to their size and weight. As known from literature dispersed gold nanoparticles may be obtained by treatment of gold with intense lasers pulses in solvents [Henglein, 1993]. In SLAB the solvents are required first to form the alkanethiol reservoir on the surface, and second to disperse the formed gold nanoparticles and preventing them to contaminate the surface. By gold patterning through a thin layer of solvent like ethanol a clean surface is obtained while the generated gold particles are dispersed in the fluid phase.

At the time when pure water or water soluble thiols are used (i. e. cysteine) in the structuring process the SLAB method is biocompatible. For example it is possible to first immobilize PM on a structured SAM while performing subsequent patterning steps by SLAB without damaging the PMs. Furthermore, the feature size of patterns generated with SLAB is in the micron range which fits well to the dimension of PM.

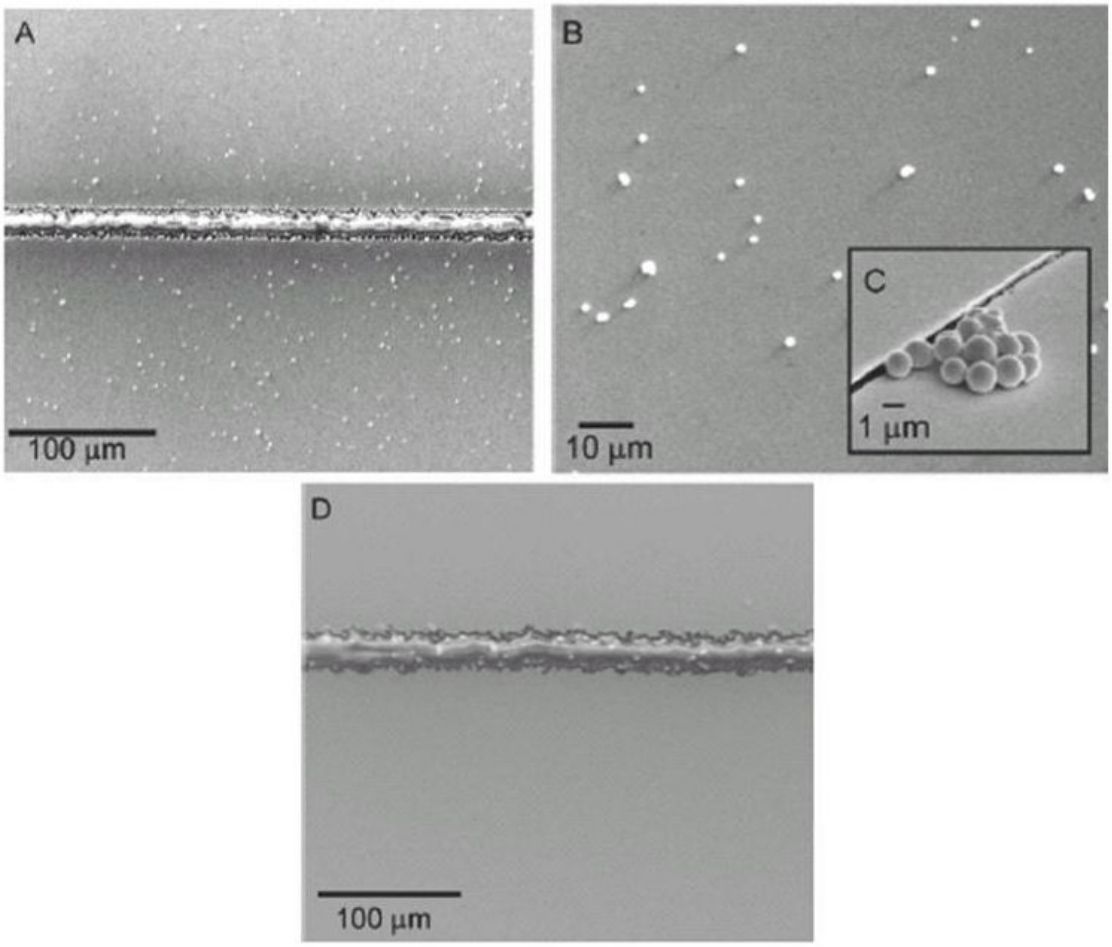

Figure 23 The SLAB process drastically reduces contamination: A) Laser ablation of gold in air causes contamination like spherical gold particles, which are found all over the surface. As the SAMs formed have a thickness of only a few nanometers, micrometer-sized contamination (B and C) are intolerable. D) By employing SLAB, where a layer of water or organic solution is placed on top of the substrate, any surface contamination with gold particles from the ablation process, but also with dust particles from the environment, is avoided.

By gold patterning through a thin layer of solvent like ethanol a clean surface is obtained while the generated gold particles are dispersed in the fluid phase. In figure 23 the structuring of a gold substrate is shown which carries a DT SAM. The horizontal line in Fig. 23A was prepared by laser ablation of gold including the DT SAM in air. A lot of small particles covering the whole surface are seen. Figures 23B and 23C are close ups of

the particles which have a diameter of about 1 µm. In Fig. 23D the same process is shown, but the DT SAM on gold was covered with a layer of ethanol. No particles on the surface are observed. The gold nano- and microparticles would cause electrical shortcuts, e.g., in cases where the patterned monolayers are used in electrochemical sensors.

3.2.3.3. Analysis of patterned SAMs by Cyclic voltammetry

The electrochemical properties of SAM coated TSG samples were analyzed before and after SLAB patterning. Retention of the insulating properties of the SAMs during the patterning procedure was verified by cyclic voltammetry (CV). In figure 24 the CV current-potential (I-E) curves for a DT SAM on gold before (red) and after SLAB processing (black) are shown with bare gold (green) as a reference. For the SAM coated TSG merely capacitive currents are observed. This property did not change after processing the sample by SLAB. This is a strong indication for the retention of the SAM's high insulation and in turn its density.

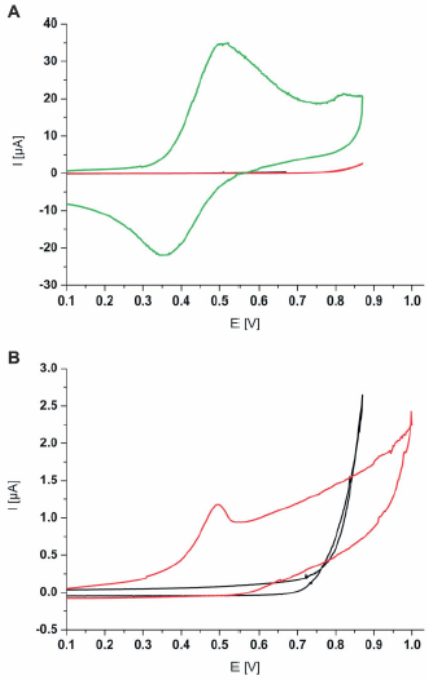

Figure 24 The insulating properties of the SAM on TSG stay intact during the SLAB process. A) Cyclic voltammetry (CV) of a DT SAM on TSG before (red) and after gold/SAM patterning (black). CV of bare gold (green) is shown as reference. B) CV of a DT-coated gold substrate (black) and after preparing an area of bare gold (1 mm * 1 mm) by the SLAB process.

3.3. Mechanics of freely-suspended purple membranes

3.3.1. Light-induced bending of purple membranes analyzed by cryo-SEM

PM-WT and PM-D96N were chosen to distinguish between the two alternative models which have been proposed to be responsible for transient purple membrane bending, that is the proton transport-dependent electrogenic [Czege, Rheinisch, 1991] versus the BR M-state shape-related mechanical hypothesis [Porschke, 2003]. PM-WT is efficient in proton pumping while not accumulating M-state due to the short M-lifetime in the range of 10 ms, whereas D96N is less efficient in proton pumping, but accumulates the late M-state (M_2-state) during photocycle, in particular at higher pH-values. Therefore, electrogenic effects due to charge separation would dominate the photoycle of PM-WT, while accumulation of the M_2-state during the photocycle of PM-D96N would impose mechanical stress to the membrane due to large-scale conformational changes.

.Figure 25A shows patches of PM-WT, fast-frozen in buffered suspension (pH = 9) in the absence of light, followed by freeze-etch, and sublimation of surface-bound-ice. The membranes appear as flat disks, most of them with rather round contours. From that follows that adsorption of PM to a flat support (*i.e.* in the case of AFM and electron crystallography) does not cause topological artifacts to PM because the flat topology resembles the topology of freely-suspended PM. That is of rather importance because in *Halobacterium salinarum* PM patches are all bent, due to the geometrical constraints of the cell [Stockenius et al., 1979], but obviously they prefer a rather flat topology when freely-suspended in solution.

Interestingly, no evidence was found for bending due to illumination of PM-WT. The membrane patches resemble those observed in the non-illuminated preparations. Figure 25B shows a cryo-SEM image of a PM fast-frozen under continuous illumination. It is concluded that under steady-state illumination electrogenic effects would not induce bending of PM-WT, at least not to degrees sufficient for detection by cryo-SEM. This observation matches results of a recent x-ray scattering study performed with BR incorporated into phospholipid membranes [Giahi et al., 2007]. The authors investigated fluctuations driven by active membrane proteins but could not detect any illumination-dependent changes in the scattering curves for membrane-embedded PM-WT.

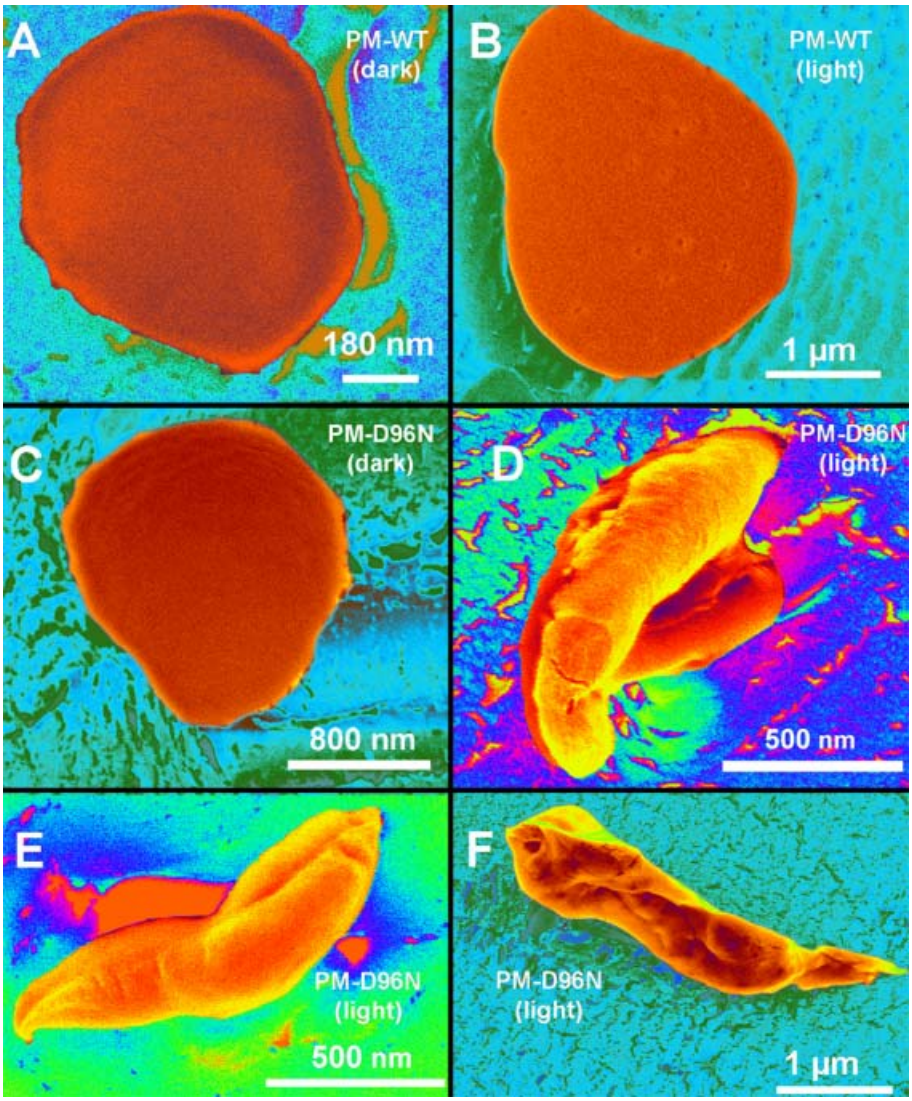

Figure 25 Illumination-dependent topology of PM analyzed by cryo-SEM (A) PM-WT (pH = 9), nonilluminated. (B) PM-WT (pH=9), fast-frozen under continuous illumination. (C) PM-D96N (pH = 9), nonilluminated. (D), (E), and (F) PM-D96N (pH = 9), fast-frozen under continuous illumination

A completely different picture arises when mutant PM-D96N is analyzed under the same preparation conditions. Patches of non-illuminated PM-D96N appear flat (Fig. 25C) whereas twisted membranes are observed in samples, frozen under steady-state illumination conditions (Fig. 25D). Typical membranes comprise twisted structures, and show irregular deformations. These observations clearly support the mechanical hypothesis which was put forward for purple membrane bending [Porschke, 2003].

Obviously, large-scale conformational changes in the M_2-state are responsible for considerable changes in PM topology during the photocycle. The shape of light-exposed PM-D96N depends on the percentage of molecules in the M_2-state.

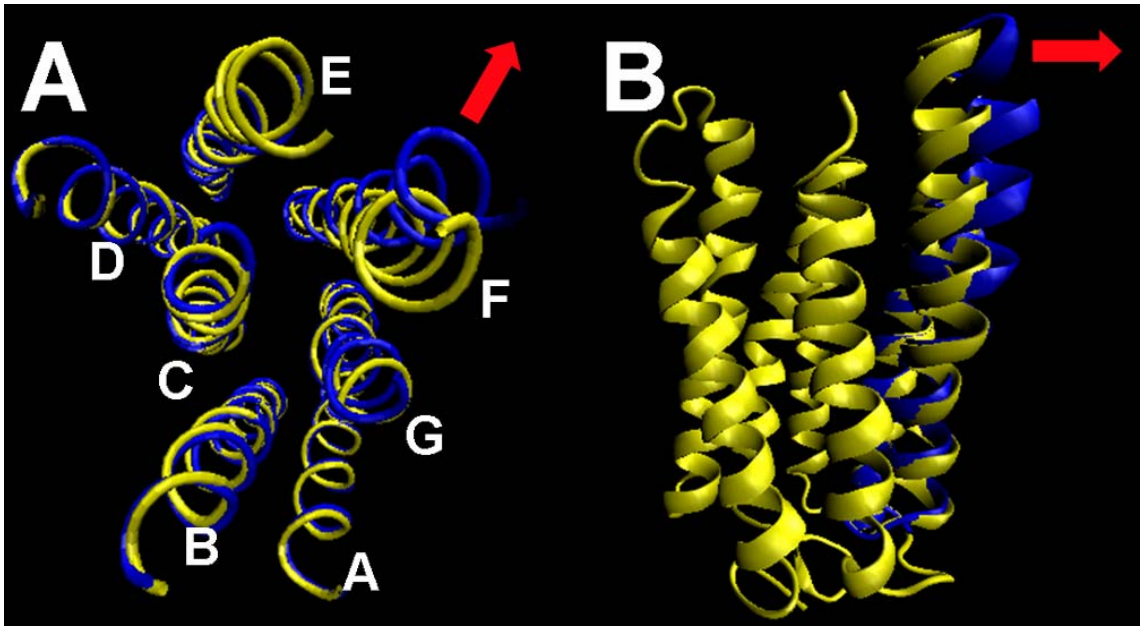

Figure 26 Large-scale conformational changes between the initial B-state and the M_2-state. (A) Alignment of B-state BR (yellow) and BR in M_2-state (blue), seen from the CP side. BR transmembrane helixes are labeled A-G. Coordinates were obtained from PDB entries 1FBB and 1FBK. (B) The Outward tilt of helix F (red arrow) leads to wedge-shaped BR. Structures were built using the program VMD [Humphrey et al., 1996].

Local conformational changes in protein structure (Fig. 26) induce large-scale changes in membrane curvature. Light excitation of BR is followed by a sequence of photocycle intermediates which comprise distinct conformations of chromophore and protein scaffold [Haupts et al., 1999]. While the initial rearrangements go along with only minor changes in the protein framework, a large-scale conformational change occurs, when the CP half-channel opens in the M_2-state [Subramaniam et al., 1999; Sass et al., 1997]. Protein structural analysis has given strong evidence for large movements within helixes F and G, accompanied by a considerable outward tilt of helix F in the M_2-state [Subramaniam, Henderson, 2000; Subramaniam et al., 1999; Sass et al., 1997]. In Fig. 26A the structural model of the M_2-state (blue molecule, PDB-entry 1FBK) is aligned with the B-state (yellow, PDB-entry 1FBB), as seen from the CP side. The outward tilt of the CP part of

helix F (red arrows in Fig.26) leads to a wedge-like structure of BR (Fig.26B) which will cause membrane bending.

Wedge-shaped proteins are able to induce strong membrane curvature. Recent examples are integral membrane proteins from the endoplasmatic reticulum which produce highly-curved membrane structures *in vivo* and *in vitro* [Hu et al., 2008].

Continuous-light illumination of PM-D96N leads to accumulation of wedge-shaped BR molecules due to the largely prolonged life-time of the M_2-state, and the membrane assembly will relax into a strongly bent form.

3.3.2. pH-induced bending of mutant D85T

In the light of the results discussed in the previous paragraph the light-dependent investigations were complemented by pH-dependent experiments.
Aspartic acid 85 is the primary proton acceptor of the protonated Schiff base in PM-WT. Replacement of D85 by a neutral residue changes the pK_a-values of other characteristic residues involved in proton translocation, and leads to different modes of ion translocation. The D85X mutants (X = neutral residue) share the property of a significantly lowered pK_a-value of the Schiff base which is >13 in non-illuminated PM-WT, but about 8-9 in the D85X mutants. [Tittor et al., 1995; Tittor et al., 1997].

It was demonstrated by x-ray diffraction studies with mutant D85N that deprotonation of the Schiff base at alkaline pH is accompanied by the same helix movements which are normally caused by M_2-state formation in the photocycle [Brown et al. 1997]. Difference maps revealed the well-known outward tilt of helix F, and gave evidence for the leading role of proton-coupled reactions in BR, even in the absence of light. The results were complemented by subsequent studies which employed solid-state NMR [Kawase et al., 2000].

Given that alkaline-mediated deprotonation of the Schiff base triggers the same conformational changes responsible for PM bending in the M_2-state, one might expect PM

bending in this case as well. Consequently, the D85X mutants offer the opportunity to study PM bending in thermal equilibrium, and to verify the mechanical model, introduced for PM bending.

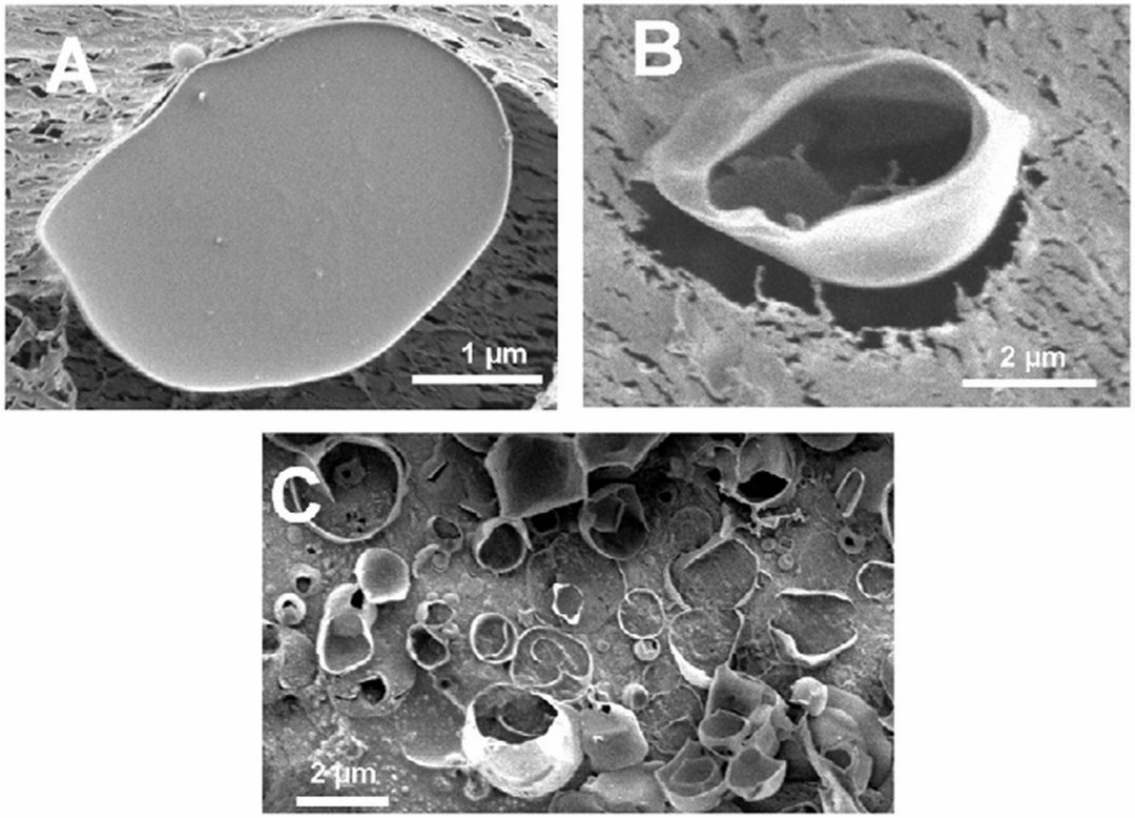

Figure 27 Conformational changes of PM-D85T in dependence on the pH. (A) Cryo-SEM image of PM-D85T observed at pH = 7 (B) and (C) PM-D85T at pH = 9. Membranes are strongly bent, forming partial spheres or are bent cylindrically, depending on the membrane geometry.

In the experiments with mutant D85T strong bending of PM was observed when raising the pH from 7 to 9 (Fig. 27B, C). At neutral pH PM-D85T appears in round disks (Fig. 27A), resembling those observed in previous experiments (Fig. 25A, B, and C). Upon alkalinization strongly bent membranes were observed (Fig. 27B). An overview image of PM-D85T (pH = 9) is given in figure 27C which shows various membranes comprising similar curvature.

These observations are fully compatible with the theoretical background outlined in the previous paragraph. Deprotonation of the Schiff base at alkaline pH triggers the outward tilt of helix F (Fig. 26A), leading to strong bending of PM, due to the wedge-shaped BR molecule (Fig. 26B). These observations support the concept of a 'deprotonation switch', responsible for the opening of the CP half-channel [Brown et al., 1997].

We have to distinguish between PM in thermodynamical equilibrium (D85T, pH = 9, dark) and active membranes, trapped 'at work', and thus under nonequilibrium conditions (D96N, steady-state illumination). Under continuous-light illumination BR molecules localized at different positions in the membrane will act independently which leads to wrinkling of PM-D96N, rather than ordinary bending, as observed with PM-D85T. Besides the mechanical stress, induced by protein conformational changes, active membranes experience forces due to the interplay of working proteins and membrane fluctuations [Prost et al. 1996; Prost et al., 1998; Manneville et al., 1999; Ramaswamy et al., 2000; Manneville et al., 2001; Gov, 2004; Lin et al. 2006; Giahi et al. 2007].

3.3.3. Mechanistic basis of purple membrane bending

Table 2 reviews the observations made and demonstrates how PM bending is coupled to the states of essential functional residues in BR which are schematically shown in Fig.28A. PM bending is observed when the Schiff base is deprotonated. This happens during M_2-state in the photocycle as well as in the case of alkaline-mediated Schiff base deprotonation in D85T (highlighted in grey in table 2).

The light-dependent experiments support the mechanical model for transient bending within the M_2-state of the photocycle. Besides the photochemical route to accumulate wedge-shaped BR, the pH-dependent experiments with D85T open the way for the study of PM bending in thermal equilibrium. The observations made with D85T give evidence for the validity of the deprotonation-switch model [Brown et al., 1997]. Deprotonation of the Schiff base triggers the opening of the CP channel, and the membranes, comprising wedge-shaped BR, relax into a highly-curved form.

	PM-WT B-state dark (light-adapted)	PM-D96N B-state dark (light-adapted)	PM-D96N M_2-state light (continuous illumination)	PM-D85T Neutral pH	PM-D85T Alkaline pH
Retinal	all-trans	all-trans	13-cis	all-trans	all-trans
Schiff base	protonated	protonated	deprotonated	protonated	deprotonated
D96	protonated	protonated	protonated	protonated	protonated
D85	anionic	anionic	neutral (protonated)	neutral (D→T)	neutral (D→T)
PM topology	flat	flat	twisted	flat	bent

Table 2 Coupling of PM topology to the protonation state of essential amino acids as well as the Schiff base linkage in BR. Because in D85T at pH = 7 the PM appears flat, but bent at pH = 9, it is concluded, that solely the Schiff base protonation state is responsible for membrane bending.

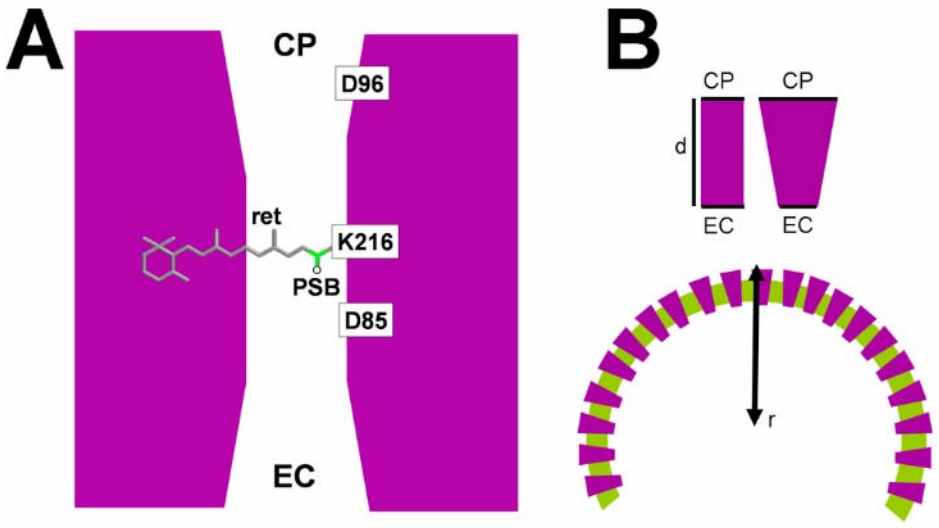

Figure 28 Scheme of PM bending. (A) Essential residues of BR involved in the photocycle. Ret: Retinal, PSB: protonated Schiff base. PM bending is coupled to the deprotonation of the PSB. In PM-D85T the proton acceptor D85 is replaced by the neutral amino acid threonine (B) Opening of the CP half-channel is accompanied by the formation of wedge-shaped BR. Due to the high protein to lipid ratio, the geometrical asymmetry is amplified through the PM crystal, and leads to PM bending. d: PM thickness, r: radius of curvature.

Light activation initiates the photocycle, and promotes the energy for the subsequent conversions, but apart from the primary photochemical step all other proton transfer-coupled reactions are thermal processes. This provides the opportunity to study the proton transfer reactions and the accompanying protein structural changes without the use of light [Lanyi, 2007].

When combined with methods for the 3-D reconstruction from SEM images [Ritter et al., 2003] cryo-SEM would allow estimating the coupling of macroscopic curvature and nanoscopic changes in individual BR molecules in a quantitative manner.

3.3.4. Membrane bending due to opening of the EC half-channel

Another event which would generate a wedge-like protein shape is the opening of the extracellular (EC) half-channel. Opening of the EC half-channel accompanies the reprotonation of the proton release complex in the O-state of the photocycle which shares structural similarities with acid blue membrane [Rouhani et al., 2001; Okumura et al., 2005]. Some years ago a 3-D structure of the mutant PM-D85S at acidic pH was obtained by x-ray crystallography and was interpreted as a model for the O-state of the photocycle [Rouhani et al., 2001]. These observations are in line with previous titration experiments with PM-D85T [Tittor et al., 1997] Therefore, the related mutant PM-D85T provides the opportunity to study the effect large-scale conformational changes in the extra cellular region of PM, thus completing the picture for membrane bending of PM-D85T (Fig. 29A).

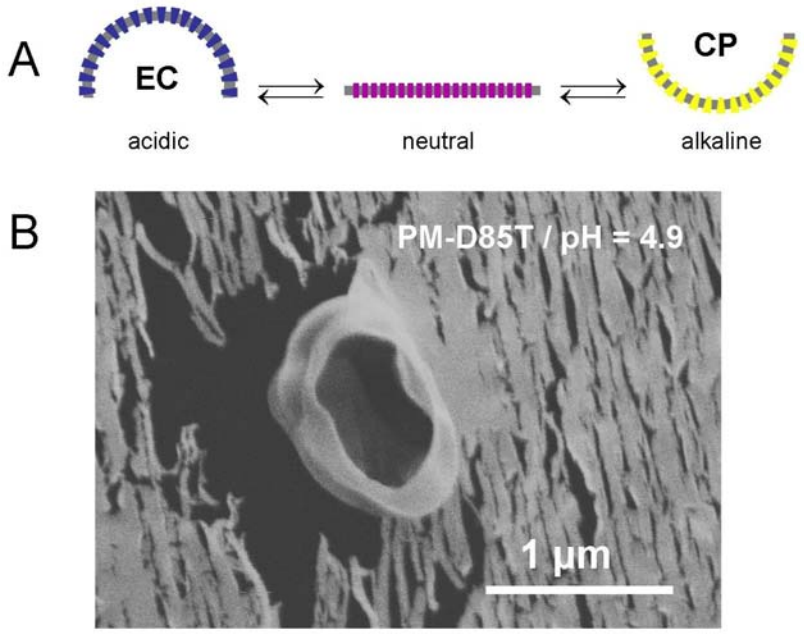

Figure 29 Generalized model for pH-dependent bending of PM-D85T. (A) At acidic pH the structure of D85T resembles the O-state of BR (all EC half-channels are open). At alkaline pH all CP half-channel open. The membranes are found in an intermediate state at pH = 7 (flat topology). (B) cryo-SEM image of PM-D85T, fast-frozen at pH = 4.9.

Indeed, bent membranes were observed when PM-D85T was fast-frozen at pH = 4.9 (Fig. 29B). This demonstrates that different bending modes are observed with mutant PM-D85T, depending on the pH value chosen. To give further evidence to this hypothesis, methods have to be employed which are suitable to detect the absolute sidedness of the membrane surfaces.

Besides the routes discussed above, all processes which involve accumulation of wedge-shaped BR monomers would induce PM bending. For example, opening of the CP half-channel continues within the N-state of the photocycle [Vonck, 2000], and BR mutants have been described which permanently assume an M_2-like conformation without illumination [Subramaniam, Henderson, 2000; Tittor et al., 2002]. Furthermore, it has been followed from spectroscopic studies that chromophor removal triggers conformational changes analogous to the M_2-state [Ludlam, Rothschild, 1997].

3.3.5. The purple membrane is a supramolecular actuator

Nanometer-scaled conformational changes in the BR monomer generate mechanical forces which add up through the large number of strongly coupled proteins comprising PM, and finally lead to changes on the micron scale. In turn, membrane curvature is a macroscopic parameter that can be analyzed by cryo-SEM, and can be utilized to estimate the state of single protein molecules.

In the case of devices which employ matrix-embedded as well as solid-supported PM, the bending behavior must seriously be taken into account. From the viewpoint of nanobiotechnology, PM is a supramolecular actuator, set in motion by changes in illumination or pH, depending on the mutant used. This puts PM into the context of other molecular machines and supramolecular switches [Skehel et al., 1982; Carr et al., 1992; Noji et al., 1997; Shingyoji et al., 1998; Mao et al., 1999; Mahadevan, Matsudaira, 2000; Itoh et al., 2004], and widens the field of potential applications of PM.

References

Anderson, M. E.; Mihok, M.; Tanaka, H.; Tan, L.-P; Horn, M. W.; McCarty, G. S.; Weiss, P. S. *Adv. Mater.* **2006**, *18*, 1020.

Angyal, S. J. *Chem. Soc. Rev.* **1981**, *11*, 415.

Angyal, S. J. *Adv. Carbohydr. Chem. Biochem*. **1989**, *47*, 1.

Arrondo, J. R.; Castresana, J. M.; Valpuesta, J. M.; Goni, F. M. *Biochemistry* **1994**, *33*, 11650.

Banks, J. T.; Yu, T. T.; Yu, H. Z. *J. Phys. Chem. B* **2002**, *106*, 3538.

Bauer, M.; Pelkmans, L. *FEBS Lett.* **2006**, *580*, 5559.

Behm, J. M.; Lykke, K. R.; Pellin, M. J.; Hemminger, J C. *Langmuir* **1996**, *12,* 2121.

Birge, R. R.; Govender, D. S. K.; Izgi, K. C.; Tan, E. H. L. J. Phys. Chem. **1996**, *100*, 9990.

Bietsch, A.; Hegner, M.; Lang, H.-P.; Gerber, C. Langmuir **2004**, *20*, 5119.

Brouillette, C. G.; Muccio, D. D.; Finney, T. K. *Biochemistry* **1987**, *26*, 7431.

Brown, L.; Kamikubo, H.; Zimányi, L.; Kataoka, M.; Tokunaga, F.; Verdegem, P.; Lugtenburg, J.; Lanyi, J. K. *Proc. Natl. Acad. Sci. USA* **1997**, *94*, 5040.

Carninci, P.; Nishiyama, Y.; Westover, A.; Itoh, M.; Nagaoka, S.; Sasaki, N.; Okazaki, Y.; Muramatsu, M.; Hayashizaki, Y. *Proc. Natl. Acad. Sci. USA.* **1998**, *95*, 520.

Carpenter, J. F.; Crowe, L. M.; Crowe, J. H. *Biochim. Biophys. Acta* **1987**, *923*, 109.

Carr, C. M.; Chaudry, C.; Kim, P. S. *Proc. Natl. Acad. Sci. U.S.A.* **1997**, *94*, 14306.

Chang, C.-H.; Chen, J. G.; Govindjee, R.; Ebrey, T. *Proc. Natl. Acad. Sci. USA.* **1985**, *82*, 396.

Chang, C.-H.; Jonas, R.; Melchiore, S.; Govindjee, R.; Ebrey, T. G. *Biophys J.* **1986**, *49*, 731.

Cladera, J.; Galisteo, M. L.; Dunach, M.; Mateo, P. L.; Padros, E. *Biochim. Biophys. Acta* **1988**, *943*, 148.

Cladera, J.; Sabes, M.; Padros, E. *Biochemistry* **1992**, *31*, 12363.

Crowe, J. H.; Crowe, L. M.; Chapman, D. *Science* **1984**, *223*, 701.

Crowe, J. H.; Hoekstra, F. A ; Crowe, L. M. *Annu. Rev. Physiol.* **1992**, *54*, 579.

Czege, J.; Rheinisch, L. *Acta Biochim. Biophys. Hung.* **1987**, *22*, 463.

Czege, J.; Rheinisch, L. *Photochem. Photobiol.* **1991**, *54*, 923.

Dameron, A. A.; Hampton, J. R.; Smith, R. K.; Mullen, T. J.; Gillmor, S. D.; Weiss, P. S. *Nano Lett.* **2005**, *5*, 1020.

Davis, F.; Higson, S. P. J. *Biosens. Bioelectr.* **2005**, *21*, 1.

Drickamer, K. *Curr. Opin. Struct. Biol.* **1999**, *9*, 585.

Druckmann, S.; Ottolenghi, M.; Pande, A.; Callender; R.H. *Biochemistry* **1982**, *21*, 4953.

Dubochet, J.; Adrian, M.; Chang, J. J; Homo, J. C.; Lepault, J.; McDowall, A. W.; Schultz, P. *Q. Rev. Biophys.* **1988**, *21*, 129.

Eliash, T.; Weiner, L.; Ottolenghi, M.; Sheves, M. *Biophys. J.* **2001**, *81*, 1163.

Essen, L.-O.; Siegert, R.; Lehmann, W. D.; Oesterhelt., D. *Proc. Natl. Acad. Sci. USA.* **1998**, *95*, 11673.

Farsad, K.; De Camilli, P.; *Curr. Opin. Cell. Biol.* **2003**, *15*, 372.

Fenimore, P. W.; Frauenfelder, H.; McMahon, B. H.; Parak, F. G. *Proc. Natl. Acad. Sci. USA.* **2002**, *99*, 16047.

Ferrer, M. L.; Garcia-Carvajal, Z. Y.; Yuste, L.; Rojo, F.; del Monte, F. *Chem. Mater.* **2006**, *18*, 1458.

Fischer, T.; Hampp, N. A.; *Biophys J.* **2005**, *89*, 1175.

Fischer, U. C.; Towner, P.; Oesterhelt, D. *Photochem. Photobiol*. **1981**, *33*, 529.

Fitter, J.; Lechner, R. E.; Büldtt, G.; Dencher, N. A. *Proc Natl. Acad. Sci. USA* **1996**, *93*, 7600.

Fraunfelder, H.; Fenimore, P. W.; Chen, G.; McMahon, B. H. *Proc. Natl. Acad. Sci. USA.* **2006**, *103,* 15469.

Fura, A.; Leary, J. A. *Anal. Chem.* **1993,** *65*, 2805.

Ganea, C.; Gergely, C.; Ludmann, K.; Váro, G. *Biophys J.* **1997**, *73*, 2718.

Ge, H.; Zhao, C.-L.; Porzio, S.; Zhuo, L.; Davis, H. T.; Scriven, L. E. *Macromolecules* **2006**, *39*, 5531.

Giahi, A.; El Alaoui, M.; Bassereau, P.; Salditt, T. *Eur. Phys. J. E* **2007**, *23*, 431.

Gölzhäuser, A.; Eck, W.; Geyer, W.; Stadler, V.; Weimann, T.; Hinze, P.; Grunze, M. *Adv. Mater.* **2001**, *13*, 806.

Gonen, T.; Cheng, Y.; Sliz, P.; Hiroaki, Y.; Fujiyoshi, Y.; Harrison, S. C.; Walz, T. *Nature* **2005**, *438, 633.*

Gov, N. *Phys. Rev. Lett.* **2004**, *93,* 268104.

Grigorieff, N.; Ceska, T. A.; Downing, K. H.; Baldwin, J. M; Henderson, R. *J. Mol. Biol.* **1996**, *259*, 393.

Hagen, S. J.; Hofrichter, J.; Eaton, W. A. *Nature* **1995**, *269*, 959.

Hampp, N. *Chem. Rev.* **2000**, *100*, 1755.

Harder, P.; Grunze, M.; Dahint, R.; Whitesides, G. M.; Laibinis, P. E. *J. Phys. Chem. B* **1998**, 102, 426.

Harte, W. E.; Bajorath, J. *J. Am. Chem. Soc.* **1994**, *116*, 10394.

Haupts, U.; Tittor, J.; Oesterhelt, D. *Ann. Rev. Biophys. Biomol. Struct.* **1999**, *28*, 367.

Heister, K.; Zharnikov, M.; M. Grunze, *Langmuir* **2001,** *17,* 8.

Henderson, R.; Baldwin, J. M.; Ceska, T. A.; Zemlin, F.; Beckmann, E.; Downing, K. H. *J. Mol. Biol.* **1990**, *213*, 899.

Henglein, A. *J. Phys. Chem.* **1993**, *97*, 5457.

Heyes, C. D.; El-Sayed, M. A. *Biochemistry* **2001**, *40*, 11819.

Hofmeister, G. E.; Zhou, Z.; Leary, J. A. *J. Am. Chem. Soc.* **1991**, *113*, 5964.

Hu, J.; Shibata, Y.; Voss, C.; Shemesh, T.; Zongli, L.; Coughlin, M.; Kozlov, M. M.; Rapoport, T. A.; Prinz, W. A. *Science* **2008**, *319*, 1247

Huang, J.; Dahlgren, D. A.; Hemminger, J. C. *Langmuir* **1994**, *10*, 626.

Itoh, H.; Takahashi, A.; Adachi, K.; Noji, H.; Yasuda, R.; Masasuke, Y.; Kinosita Jr, K. *Nature* **2004**, *427*, 465.

Jackson, M. B.; Sturtevant, J. M. *Biochemistry* **1978**, *17*, 911.

Jonas, R.; Ebrey. T. G. *Proc. Natl. Acad. Sci. U.S.A.* **1991**, *88*, 149.

Kandori, H. *Biochem. Biophys. Acta* **2000**, *1460*, 177.

Kaushik J. K.; Bhat, R. *J. Biol. Chem*. **2003**, *278*, 26458.

Kawase, Y.; Tanio, M.; Kira, A.; Yamaguchi, S.; Tuzi, S.; Naito, A.; Kataoka, M.; Lanyi, J. K.; Needleman, R.; Saito, H. *Biochemistry* **2000,** *39,* 14472.

Kimura, Y.; Ikegami, A.; Stoeckenius W. Photochem. Photobiol. **1984**, *40*, 641.

Kimura, Y.; Vassylyev, D. G.; Miyazawa, A.; Kidera, A.; Matsushima, M.; Mitsuoka, K.; Murata, K.; Hirai, T.; Fujiyoshi, Y. *Nature* **1997**, *389*, 206.

Koltover, I.; Salditt, T.; Rigaud, J.-L.; Safinya, C. R. *Phys. Rev. Lett.* **1998**, *81*, 2494.

Koltover, I.; Raedler, J. O.; Salditt, T.; Rothshild, K. J.; Safinya, C. R. *Phys. Rev. Lett.* **1999**, *82*, 3184.

Korenstein, R.; Hess, B. *Nature* **1977**, *270*, 184.

Kühlbrandt, W.; Wang, D.N.; Fujiyoshi, Y. *Nature* **1994**, *367*, 614.

Kuehnle, A.; Linderoth, T. R.; Hammer, B.; F. Besenbacher, *Nature* **2002**, *415*, 891.

Kumar, A.; Whitesides, G. M. *Appl. Phys. Lett.* **1993**, *63*, 2002.

Lanyi, J. K. *J. Mol. Microbiol. Biotechnol.* **2007**, *12*, 210.

Lemoine, J.; Strecker, G.; Leroy, Y.; Fournet, B.; Ricart, G. *Carbohydr. Res.* **1991**, *221*, 209.

Lercel, J.; Redinbo, G. F.; Pardo, F. D.; Rooks, M.; Tiberio, R. C.; Simpson, P.; Craighead, H. G.; López, G. P.; Biebuyck, H. A.; Whitesides, G. M. *Langmuir* **1993**, *9*, 1513.

Liang, G.; Schmidt, R. K.; Yu, H. A.; Cumming, D. A.; Brady, J. W. *J. Phys. Chem.* **1996**, *100*, 2528.

Lin, L. C.-L.; Gov, N.; Brown, F. L. H.; *J. Chem. Phys.* **2006**, *124*, 074903.

Liu, S. Y.; Ebrey, T. G. *Photochem. Photobiol.* **1987**, *46*, 557.

López, G. P.; Biebuyck, H. A.; Whitesides, G. M. *Langmuir* **1993**, *9*, 1513.

Love, J. C.; Estroff, L. A.; Kriebel, J. K.; Nuzzo, R. G.; Whitesides, G. M. *Chem. Rev.* **2005**, *105*, 1103.

Luecke, H.; Schobert, B.; Richter, H.-T.; Cartailler, J.-P.; Lanyi, J. *J. Mol. Biol*. **1999**; *291*, 899.

Luecke, H. *Biochem. Biophys. Acta* **2000**, *1460*, 133.

Ludlam, G.; Rothschild, K. J. *FEBS Lett.* **1997**, *407*, 285.

MacDairmid, A. R.; Gallagher, M. C.; Banks, J. T. *J. Phys. Chem. B* **2003**, *107*, 9789.

Mahadevan, L.; Matsudaira, P. *Science* **2000**, *288*, 95.

Manneville, J.-B. ; Bassereau, P.; Lévy, D.; Prost, J. *Phys. Rev. Lett.* **1999**, *82*, 4356.

Manneville, J.-B.; Bassereau, P.; Ramaswamy, S.; Prost, J. *Phys. Rev. E* **2001**, *64*, 021908.

Mao, C.; Sun, W.; Shen, Z.; Seeman, N. C. *Nature* **1999**, *397*, 144.

Martens, S.; Kozlov, M. M.; McMahon, H. T. *Science* **2007**, *316*, 1205.

Masthay, M. B.; Sammeth, D. M.; Helvenston, M. C.; Buckman, C. B.; Li, W.; Cde-Baca, M. J.; Kofron, J. T. *J. Am. Chem. Soc.* **2002**, *124*, 3418.

Menger, F. M.; Zhang, H.; Caran, K. L.; Seredyuk, V. A.; Apkarian, R. P. *J. Am. Chem Soc.* **2002**, *124*, 1140.

Menger, F.M.; Seredyuk, V. A.; Apkarian, R. P.; Wright, E. R. *J. Am. Chem Soc.* **2002**, *124*, 12408..

Menger, F. M.; Galloway, A. L.; Chlebowski, M. E.; Apkarian, R. P. *J. Am. Chem. Soc.* **2004**, *126*, 5987.

Mowery, P. C.; Lozier, R. H.; Chae, Q.; Tseng, I. W.; Taylor, M.; Stoeckenius, W. *Biochemistry* **1979**, *18*, 4100.

Müller, D. J.; Büldt, G.; Engel, A.. *J. Mol. Biol.* **1995**, *249*, 239.

Müller, D. J.; Engel., A. *J. Mol. Biol.* **1999**, *285*, 1347.

Müller, D. J.; Sass, H.-J.; Müller, S.; Büldt, G. Engel., A. *J. Mol. Biol.* **1999**, *285*, 1903.

Müller, D. J.; Fotiadis, D.; Scheuring, S.; Müller, S. A.; Engel, A. *Biophys J.* **1999**, *76*, 1101.

Müller, J.; Münster, C.; Salditt, T. *Biophys. J.* **2000**, *78,* 3208.

Neebe, M.; Rhinow, D.; Schromczyck, N.; Hampp, N. *J. Phys. Chem. B* **2008**, *112*, 6946.

Noji, H.; Yasuda, R.; Yoshida, M.; Kinosita Jr, K. *Nature* **1997**, *386*, 299.

Oesterhelt, D.; Stoeckenius, W. *Nat. New Biol.* **1971**, *233*, 149.

Oesterhelt, D.; Meentzen, M.; Schuhmann, L. *Eur. J. Biochem.* **1973**, *40,* 453.

Oesterhelt, D.; Stoeckenius, W. *Methods Enzymol.* **1974**, *31*, 667.

Oesterhelt, F.; Oesterhelt, D.; Pfeiffer, M.; Engel, A.; Gaub, H.;. Müller, D. J. *Science* **2000**, *288*, 143.

Okumura, H.; Murakami, M.; Kouyama, T.; *J. Mol. Biol.* **2005**, *351*, 481.

Orford, P. D.; Parker, R.; Ring, S. G. *Carbohydr. Res.* **1990**, *196*, 11.

Pande, C.; Callender, R.; Henderson; R. Pande, A. *Biochemistry* **1989**, *28*, 597.

Padros, E.; Duñach, M.; Sabés, M. *Biochim. Biophys. Acta* **1984**, *769*, 1.

Pardo, L.; Wilson Jr, W. C.; Boland, T. *Langmuir* **2003**, *19*, 1462.

Patzelt, H.; Simon, B.; TerLaack, A.; Kessler, B.; Kühne, R.; Schmieder, P.; Oesterhelt, D.; Oschkinat, H. *Proc. Natl. Acad. Sci. USA* **2002**, *99*, 9765.

Piner, R. D.; Zhu, J.; Xu, F.; Hong, S.; Mirkin, C. A. *Science* **1999**, *283*, 661.

Porschke, D.; *J. Mol Biol.* **2003**, *331*, 667.

Prost J.; Bruinsma, R. *Europhys. Lett.* **1996**, *33*, 321.

Puzo, G.; Fournie, J. J.; Prome, J. C. *Anal. Chem.* **1985**, *57*, 892.

Ramaswamy, S.; Toner, J.; Prost, J. *Phys. Rev. Lett.* **2000**, *84,* 3494.

Renthal, R.; Gracia, N.; Regalado, R. *Photochem. Photobiol.* **2000**, *72*, 714.

Rhinow, D.; Hampp, N. *IEEE Trans. Nanobiosci.* **2006**, *3*, 188.

Rhinow, D.; Hampp, N. A. *J. Phys Chem B* **2007**, *112*, 4613.

Rhinow, D.; Hampp, N. A. *Adv. Mater.* **2007**, *19*, 1967.

Rhinow, D.; Hampp, N. A. *J. Phys Chem. B.* **2008***, in press, published on web at 08/20/2008.*

Ritter, M.; Simram, O.; Albertz, J.; Hohenberg, H. *Microsc. Microanal.* **2003**, *9*, 476.

Roos, Y. *Carbohydr. Res.* **1993**, *238*, 39.

Rouhani, S.; Cartailler, J. P.; Facciotti, M. T.; Walian, P.; Needleman R.; Lanyi J. K.; Glaeser R. M.; Luecke, H. *J. Mol. Biol.* **2001**, *313*,615.

Salaita, K.; Wang, Y.; Fragala, J.; Vega, R. A.; Liu, C.; Mirkin, C. A. *Angew. Chem. Int. Ed.* **2006**, *45*, 7220.

Salditt, T. *Curr. Opin. Coll. Int. Sci.* **2000**, *5*, 19.

Salditt, T.; Münster, C.; Lu, J.; Vogel, M.; FenzI, W.; Souvorov, A. *Phys. Rev. E* **1999**, *60*, 7285.

Sapra, K. T.; Besir, H.; Oesterhelt, D.; Müller, D. J. *J. Mol. Biol.* **2006**, *355*, 640.

Sass, H. J.; Schachowa, I. W.; Rapp, G.; Koch, M. H. J.; Oesterhelt, D.; Dencher, N. A., Büldt, G. *EMBO J*. **1997**, *16*,. 1484.

Sass, H. J.; Büldt, G.; Gessenich, R.; Hehn, D.; Neff, D.; Schlesinger, R.; Berendzen, J; Ormos, P. *Nature* **2000**, *406*, 649.

Shadnam, M. R.; Kirkwood, S. E.; Fedosejevs, R.; Amirfazli, A. *Langmuir* **2004**, *20*, 2667.

Sheen, C. W.; Parikh, A. N.; Allara, D. L. *J. Vac. Sci. Technol. B* **1994**, *12*, 3663.

Shen, Y.; Safinya, C. R.; Liang, K. S.; Ruppert, A. F.; Rothschild, K. J. *Nature* **1993**, *366*, 48.

Sheriff, S.; Chang, C. Y. Y.; Ezekowitz, R. A. B. *Nat. Struct. Biol*. **1994**, *1*, 789.

Shingyoji, C.; Higuchi, H.; Yoshimura, M.; Katayama, E. ; Yanagida, T. *Nature* **1998**, *393*, 711.

Singer, M. A.; Lindquist, S. *Trends Biotechnol.* **1998**, *16*, 460.

Skehel, J. J.; Bayley, P. M.; Brown, E. B.; Martin, S. R.; Waterfield, M. D.; Whites, J. M.; Wilson, I. A.; Wiley, D. C. *Proc. Natl. Acad. Sci. U.S.A.* **1982**, *79*, 968.

Sonoyama, M.; Mitaku, S. *J. Phys. Chem. B* **2004**, *108*, 19496

Stoeckenius, W.; Lozier, R. H.; Bogomolni, R. A. *Biochim. Biophys. Acta* **1979**, *505*, 215.

Subramaniam, S.; Gerstein, M.; Oesterhelt, D.; Henderson, R. *EMBO J* **1993**, *12*, 1.

Subramaniam, S.; Henderson, R. *Nature* **2000**, *406*, 653.

Sun, S.; Chong, K. S. L.; Leggett, G. J. *J. Am. Chem. Soc.* **2002**, *124*, 2002.

Szundi, I.; Stoeckenius, W. *Biophys. J.* **1989**, *56*, 369.

Taneva, S. G.; Caaveiro, J. M. M.; Muga, A.; Coni, F. M. *FEBS Lett.* **1995**, *367*, 297.

Tittor, J.; Oesterhelt, D.; Bamberg, E. *Biophys. Chem.* **1995**, *56*, 153.

Tittor, J.; Haupts, U.; Haupts, C.; Oesterhelt, D.; Becker, A.; Bamberg, E. *J. Mol. Biol.* **1997**, *271*, 405.

Tittor, J.; Paula, S.; Subramaniam, S.; Heberle, J.; Henderson, R.; Oesterhelt, D. *J. Mol. Biol.* **2002,** *319*, 555.

Thompson, C. *Science* **1995**, *269*, 301.

Tuzi, S.; Yamaguchi, S.; Tanio, M.; Konishi, H.; Inoue, S.; Naito, A.; Needleman, R.; Lanyi, J. K.; Saito, H. *Biophys. J.* **1999**, *76,* 1523.

Valiokas, R.; Vaitekonis, S.; Klenkar, G.; Trinkujnas, G.; Liedberg, B. *Langmuir* **2006,** *22,* 3456.

Voeltz, G. K.; Prinz, W. A.; Shibata, Y.; Rist, J. M.; Rapoport, T. A. *Cell* **2006**, *124*, 573.

Voeltz, G. K.; Prinz, W. A. *Nat. Rev. Mol. Cell. Biol.* **2007**, *8*, 258.

Vonck J. *EMBO J.* **2000**, *19*, 2152.

Wagner, P.; Hegner, M.; Guentherodt, H.-J.; Semenza, G. *Langmuir* **1995**, *11*, 3867.

Waldeck, D.H.; Alivisatos, A. P.; Harris, C. B. *Surf. Sci.* **1985**, *158*, 103.

Weis, W. I.; Drickamer, K.; Hendrickson, W. A. *Nature* **1992**, *360*, 127.

Whitfield, D. M.; Stojkovski, S.; Sarkar, B. *Coord. Chem. Rev.* **1993**, *122*, 171.

Wong, C. H. S.; Siua, F. M.; Mab, N. L.; Tsanga, C. W. *J. Mol. Struct.* **2001**, *536*, 227.

Xu, S.; Miller, S.; Laibinis, P. E.; Liu, G. *Langmuir* **1999**, *15,* 7244.

Yang, D.; El-Sayed, M. A. *Biophys. J.* **1995**, *69*, 2056.

Zhang, Y. N.; Sweetman, L. L.; Awad, E. S.; El-Sayed., M. A. *Biophys. J.*, *1992*, *61*,1201.

Zhang, Y. N.; El-Sayed, M. A.; Bonet, M. L.; Lanyi, J. K.; Chang, M.; Ni, B.; Needleman, R. Proc. Natl. Acad. Sci. USA. **1993**, *90*, 1445.

Zheng, Y.-J.; Ornstein, R. L.; Leary, J. A. *J. Mol. Struct.* **1997**, *389*, 233.

Zimmerberg, J.; Kozlov, M. M. H *Nat. Rev. Mol. Cell. Biol.* **2006,** *7*, 9.

Abbreviations

AET	Aminoethanethiol
ABM	Acid blue membrane
AFM	Atomic force microscopy
BR	Bacteriorhodopsin
CFBM	Cation-free blue membrane
CP	Cytoplasmatic
Cryo-SEM	Cryogenic high resolution scanning electron microscopy
CV	Cyclic voltammetry
DA	Dark adapted
DIBM	Detergent-induced blue membrane
LA	Light adapted
DMSO	Dimethylsulfoxide
DT	Decanethiol
DTT	Dithiothreitol
E-Beam	Electron beam
EC	Extracellular
EDTA	Ethylenediamine tetraacetate
EM	Electron microscopy
EPR	Electron paramagnetic resonance
FTIR	Fourier transform infra red
GPCR	G-protein-coupled receptor
HDT	Hexadecanethiol

IR	Infrared
LIBM	Laser-induced blue membrane
Lys	L-lysine
MBP	Mannose binding protein
μCP	Microcontact printing
MHA	Mercaptohexadecanoic acid
MUA	Mercapto undecanoic acid
NMR	Nuclear magnetic resonance
OD	Optical density
PEG	Polyethylene glycol
PDB	Protein data bank
PM	Purple membrane
PSB	Protonated Schiff Base
SAM	Self-assembled monolayer
SEM	Scanning electron microscopy
SIBM	Sugar induced blue membrane
SLAB	Submerged laser ablation
TEM	Transmission electron microscopy
TSG	Template-stripped gold
UV	Ultraviolet
UV-Vis	Ultraviolet-visual
WT	Wild type

Danksagungen

Ganz besonders danke ich meinen Eltern für ihre unermüdliche Unterstützung auf allen Stufen meines Lebens.

***

Ich danke Herrn Prof. Dr. Hampp, dass er mir die Möglichkeit gegeben hat, meine Doktorarbeit im Bereich Nanobiotechnologie anzufertigen. Die interdisziplinäre Thematik meiner Arbeit und die damit verbundenen vielfältigen wissenschaftlichen Fragestellungen erlaubten es mir, Methoden und Konzepte aus den verschiedensten Gebieten der Biophysik und Physikalischen Chemie zu kombinieren und dabei meinen wissenschaftlichen Horizont grundlegend zu erweitern. Im Rahmen der International PhD School of Nanobiotechnology hatte ich Gelegenheit, die Städte Brixen, Genua, Padua und Venedig zu bereisen, wofür ich ebenfalls danke.

Meinen Büro-Kollegen Andreas Schönafinger, Michael Schranz und Jens Pudewills danke ich für die stets angenehme Arbeitsatmosphäre im Büro 2406 und die vielen anregenden Diskussionen über wissenschaftliche und politische Themen. Weiterhin danke ich Björn Heidel für viele interessante Diskussionen über die Zellbiologie und Genetik von *Halobacterium salinarum*. Ebenfalls Dank schulde ich Sven Kirchberg für vielfache Hilfe bei Computerfragen, Frank Noll für Tipps und Ratschläge rund um die Rasterkraftmikroskopie und Nina Schromczyk, die dafür sorgte, dass die Bakteriorhodopsin-Vorräte niemals ausgingen.

***

Eine Danksagung der besonderen Art möchte ich an meine Stammcafés in Marburg und Frankfurt richten. Während meiner Promotion haben sie mich jeden Abend nicht nur mit gutem Essen und Espresso versorgt, sondern auch die geeignete Atmosphäre geliefert, in der sich die aktuellen wissenschaftlichen Fragestellungen bestmöglich überdenken ließen.

Curriculum Vitae

Seit SS 2005	Promotion in Biophysikalischer Chemie an der Philipps-Universität Marburg bei Prof. Dr. Norbert A. Hampp Thema der Dissertation: "Purple membranes from *Halobacterium salinarum* as building blocks for nanobiotechnology: The importance of mechanical and thermal properties for matrix and surface applications"
2004	Diplomprüfungen in Physik mit Nebenfach Physikalische Chemie und Zusatzfach Organische Chemie. Gesamtnote: „Sehr gut"
Von WS 2002 bis SS 2004	Studentischer Mitarbeiter am Max-Planck-Institut für Biophysik in Frankfurt am Main Anfertigung der Physik-Diplomarbeit mit Schwerpunkt Biophysik bei Prof. Dr. Werner Kühlbrandt in der Abteilung Strukturbiologie (Biologische Cryo-Elektronenmikroskopie und Membranproteine) Teilnahme am Blockpraktikum "Biologische Kristallographie" in der Abteilung von Prof. Dr. Hartmut Michel.
2001	Diplom-Vorexamen Physik
2000	Diplom-Vorexamen Chemie
Ab WS 1998	Studium von Chemie, Physik und Biophysik an der Johann-Wolfgang-Goethe-Universität Frankfurt/Main.
1997-1998	Zivildienst beim Frankfurter Verband
1997	Allgemeine Hochschulreife Preis des Fonds der Chemischen Industrie für den besten Chemiker des Jahrgangs.
1996	Teilnahme an einem Auswahlseminar der Deutschen Schüler Akademie (DSA). Thema des Kurses: "Chemiegeschichte(n), Geschichte der Organischen Chemie."
1995	Landessieger bei „Jugend Forscht" im Fachgebiet Chemie
1988-1997	Besuch des Ziehengymnasiums in Frankfurt/Main.
19.08.1977	Geboren in Frankfurt/Main